

Disruption of astrocyte-dependent dopamine control in the developing medial prefrontal cortex leads to excessive grooming in mice

Francesco Petrelli^{1,11}, Tamara Zehnder^{1,11}, Anthony Laugeray¹, Sarah Mondoloni¹, Corrado Cali², Luca Pucci¹, Alicia Molinero Perez¹, Bianca Maria Bondiolotti¹, Eva De Oliveira Figueiredo¹, Glenn Dallerac³, Nicole Déglon^{4,5}, Bruno Giros⁶, Lorenzo Magrassi⁷, Jean-Pierre Mothet^{3,8}, Manuel Mamelì¹, Linda Simmler^{9,12}, and Paola Bezzi^{1,10,12}

1: Department of Fundamental Neurosciences (DNF), University of Lausanne (UNIL), CH-1005 Lausanne, Switzerland. 2: Department of Neuroscience, University of Torino, 10126 Torino (Italy). 3: Centre de Recherche en Neurobiologie et Neurophysiologie de Marseille, Aix-Marseille Université UMR7286 CNRS 13344 Marseille Cedex 15, France. 4 : Department of Clinical Neurosciences, Laboratory of Neurotherapies and Neuromodulation (LNTM), Lausanne University Hospital (CHUV) and University of Lausanne, CH-1011 Lausanne, Switzerland; 5: Neurosciences Research Center (CRN), Laboratory of Neurotherapies and Neuromodulation (LNTM), Lausanne University Hospital and University of Lausanne, CH-1011 Lausanne, Switzerland 6: Department of Psychiatry, Douglas Hospital Research Center, McGill University, Montreal, Quebec, H4H1R3, Canada. 7: Neurosurgery, Dipartimento di Scienze Clinico-Chirurgiche e Pediatriche, Università degli Studi di Pavia, Fondazione IRCCS Policlinico S. Matteo, 27100 Pavia, Italy. 8: "Biophotonics and Synapse Physiopathology" Team, UMR9188 CNRS - ENS Paris Saclay, 91405, Orsay, France. jean-pierre.mothet@u-psud.fr. 9: Department of Basic Neurosciences, University of Geneva, Rue Michel-Servet 1, 1206 Geneva, Switzerland 10: Department of Physiology and Pharmacology, Sapienza University of Rome, 00185 Rome, Italy 11: These authors contributed equally 12: Correspondence to Linda Simmler and/or Paola Bezzi.

Short title: astrocytic origin of pathological grooming

Keywords: astrocytes, VMAT2, dopamine, prefrontal cortex, grooming, OCD

Contact information

Paola Bezzi
Department of Fundamental Neurosciences
University of Lausanne
Rue du Bugnon 9
1005 Lausanne - Switzerland
Tel 0041 21 6925284
Email : paola.bezzi@unil.ch

Linda Simmler
Department of Basic Neurosciences
University of Geneva
Rue Michel-Servet 1
1211 Geneva - Switzerland
Phone: 0041 22 379 53 90
Email: linda.simmler@unige.ch

Abstract

Background: Astrocytes control synaptic activity by modulating peri-synaptic concentrations of ions and neurotransmitters including dopamine and, as such, could be involved in the modulating aspects of mammalian behavior.

Methods: We produced a conditional deletion of the vesicular monoamine transporter 2 specifically in astrocytes (VMAT2; aVMAT2cKO mice) and studied the effects of the lack of VMAT2 in PFC astrocytes on the regulation of dopamine levels, PFC circuits functions and behavioural processes.

Results We found a significant reduction of mPFC dopamine levels and excessive grooming and compulsive repetitive behaviours in aVMAT2cKO mice. The mice also develop a synaptic pathology, expressed through increased relative AMPA vs. NMDA receptor currents in synapses of the dorsal striatum receiving inputs from the mPFC. Importantly, behavioural and synaptic phenotypes have been rescued by re-expression of mPFC VMAT2 and L-DOPA treatment, showing that the deficits are driven by mPFC astrocytes that are critically involved in developmental dopamine homeostasis. By analysing human tissue samples, we found that VMAT2 is expressed in human mPFC astrocytes, corroborating the potential translational relevance of our observations in mice.

Conclusions: Our study shows that impairment of the astrocytic control of dopamine in the mPFC whose symptoms reminds of obsessive-compulsive spectrum disorders such as trichotillomania has a profound impact on circuit function and behaviours.

Introduction

Compulsive repetitive behaviours are key features of a plethora of neuropsychiatric disorders, including obsessive-compulsive disorder (OCD) and other OC-spectrum disorders such as Tourette's syndrome and trichotillomania (1-4). Little is known about the neurobiology underlying the development of compulsive behaviors at the cell level or the neuromodulators involved, but convergent neuroimaging and neurophysiological findings support a model in which abnormal cortico-striato-thalamo-cortical (CSTC) loops (5-9) play a crucial role in OCD-like symptoms. Furthermore, it is known that optogenetic activation of the prefrontal cortex (PFC) induces excessive grooming in rodents (10), and PFC dysfunction may also explain the lack of cognitive flexibility occurring in OCD patients (11-15). One neuromodulator in CSTC circuits is dopamine (DA), which may play a role in causing OCD symptoms (16-18) as it is crucially involved in stereotypical behavior (including abnormal grooming in rodents)(4) and a number of the cognitive and affective processes that can be altered in OCD. There is also strong evidence that the DAergic system plays a key role in Tourette's syndrome (16) and there might be some therapeutic role for D2 receptor blockers in OCD (19).

The current CSTC model of OCD and the hypothesis of DAergic involvement are both entirely neurocentric. However, over the last few years, a number of studies have revealed the importance of astrocytes in certain behaviors, including repetitive behavior (20-24), thus indicating that animal behavior is not a result of neuronal activity alone, but requires the coordinated activity of neurons and astrocytes. Astrocytes have functional peri-synaptic processes that are involved in reciprocal interactions with both pre- and post-synaptic neuronal terminals. The functional interactions of these tripartite synapses (25-30) require complex signalling mechanisms mediated by a wide range of membrane channels, ion pumps, transporters, and receptors, and alterations in such astrocyte synaptic functions affect synapse formation and maturation (29, 31-33) as well as behavioral and cognitive parameters (20-22). For example, selective elimination of astrocytes located in the prefrontal cortex (PFC) using an astrocyte specific toxin L- α -amino adipate (L-AA) results in mice with deficits in attentional setshifting, working memory, reversal learning (24) and, excessive self-grooming has been observed in mice lacking the glutamate transporter GLT1 (34) as well as mice with increased GABA transporter 3 (GAT-3) expression and when astrocytic calcium signalling is attenuated (35).

What is particularly intriguing in the context of OCD is that PFC astrocytes have the unique features of DAergic glial cells and are responsible for regulating DA homeostasis (36). This regulation takes place in the developing PFC and depends on vesicular monoamine transporter 2 (VMAT2), which controls monoamine oxidase B (MAOB)-dependent metabolic capacity by sequestering DA from the cytoplasm. Mice with conditional astrocytic VMAT2 (aVMAT2) deletion show increased MAOB activity and a consequent significant decrease in extra-cellular DA levels, and this hypo-DAergic state has been associated with increased basal PFC excitatory activity and deficits in behavioral flexibility (36), some of the key features of OCD-like phenotype in humans and mice (37).

The present study shows that mice carrying the astrocyte VMAT2 deletion display pathological grooming and anxiety-like behaviors that can be rescued by re-expressing VMAT2 in astrocytes of the medial PFC (mPFC) as well as with long-term L-DOPA treatment, thus indicating that mPFC astrocytic VMAT2 and appropriate DA levels during development are essential to prevent the pathological behaviors. We also found that the absence of VMAT2 in mPFC astrocytes changed the strength of corticostriatal synapses, a part of the circuitry implicated in OCD. To probe translational validity of these murine findings, we confirmed the presence of the determinants involved in the regulation of DA levels, including VMAT2, in samples of human frontal cortical tissues. These findings indicate that mPFC astrocytic VMAT2 and appropriate DA levels during development are essential to prevent the pathological OCD-like behaviors.

Results

Selective VMAT2 deletion in astrocytes triggers excessive grooming and anxiety-like behavior

As previously reported (36), we have produced a selective and inducible deletion of aVMAT2 by crossbreeding mice carrying a LoxP-flanked VMAT2 allele (VMAT2^{fllox/fllox}) (38) with mice expressing an inducible form of Cre (Cre^{ERT2}) under the promoter of hGFAP (39). The resulting mice treated with TAM from P20 to P28, and carrying the deletion of VMAT2 in astrocytes are here referred to as aVMAT2cKO mice (Supplementary Fig. 1a). In order to verify the cell-type specificity of VMAT2 gene deletion in mice, we used fluorescent R26-tdTomato^{fllox/fllox} mice (33) crossbred with Cre^{ERT2}-hGFAP or aVMAT2cKO mice and the expression of tdTomato in astrocytes revealed a recombination of about 60% of PFC astrocytes (Supplementary Fig. 1b). Although the aVMAT2cKO mice were healthy and their weight was similar to that of their control littermates (data not shown; 36), they presented some behavioural peculiarities. In a novel open-field test, aVMAT2cKO showed reduced exploration with shorter path distances and relative avoidance of the central zone of the arena, suggestive of an anxietylike behaviour (Figure 1a, 1b). Interestingly, a more in-depth analysis showed no negative correlation between both the total distance travelled and/or the time in center of arena with time spent in grooming of the aVMAT2cKO mice, thus indicating that the increased grooming does not justify their tendency of explore less (Supplementary Figure 1c,d). Indeed, the analysis of the time course of the open field revealed that the reduced exploration of aVMAT2cKO mice mainly occurs within 3 minutes of the exploration starting (Supplementary Figure 1e) when the anxiety associated to the fear for a novel environment and open space is greater (40). These signs of anxiety were confirmed by the elevated plus maze test, in which the aVMAT2cKO mice spent less time in the open arms and took longer to cross their distal parts (a riskier environment) (Figure 1c, 1d). The reduced open field activity of aVMATcKO mice prompted an ethological assessment of their behaviour, focused on grooming. aVMATcKO mice engaged in excessive grooming in both their home cages (Figure 1e) and in the open field (Figure 1f). There was a significant increase in the number of grooming bouts per unit of time (Figure 1g), and the duration of the bouts was significantly longer (Figure 1h). This over grooming activity resulted in facial/head and back hair loss developed from the age of 3-4 months (Figure 1i and 1j, and increased with age. We believe that whiskers' removal resulted from excessive self-grooming because, when the

mice were housed with their control littermates, the controls also developed large bald patches on their backs and on top of their heads, yet not on the whisker pads (Figure 1k). Taken together, these observations indicate that aVMAT2cKO mice are characterised by excessive grooming and increased anxiety, a behaviour that is typical of OCD spectrum disorders (4, 41, 42).

Loss of VMAT2 in astrocytes is associated with a strengthening of PFC-striatum transmission in MSNs

According to our previous results, the increase of basal excitatory activity in the PFC upon deletion of VMAT2 in astrocytes resulted from decreased levels of DA and the consequent disinhibition of DA input onto dopamine receptor 2 (D2R) of pyramidal cells (36). The increased excitatory transmission in the PFC regions has been suggested to be the cause of repetitive behaviors associated to OCD by potentiating cortico-striatal synaptic transmission (37). In order to explore how VMAT2-deficient astrocytes can affect striatal circuits, we investigated cortico-striatal synaptic transmission and checked whether the mPFC-dorsomedial striatum (DMS) pathway (43) may be involved in the compulsive behaviour of aVMAT2cKO mice.

This was done by injecting an adeno-associated virus (AAV8-Syn-ChrimsonR-GFP) into the mPFC, which anterogradely labelled fibre terminals in the medial part of the dorsal striatum as previously reported (43) (Figure 2a and 2b). The virus also expressed the channelrhodopsin (ChR2) ChrimsonR (44), which we used to activate specifically cortical fibres (Figure 2c). The ratio between AMPA and NMDA receptor excitatory post-synaptic currents (EPSCs) in dorsomedial putative medium-sized spiny neurons (MSNs) was used as a proxy for excitatory synaptic strength. Evaluation of the changes in the AMPAR:NMDAR current ratio (A/N ratio) in the putative MSNs in the DMS showed that it was increased in the aVMAT2cKO mice (Figures 2c and 2d), thus suggesting an increase in synaptic strength. Assessment of AMPAR-mediated currents at negative (-70 mV), reversal (0 mV), and positive potential (+40 mV) in order to test for the presence of AMPARs lacking GluA2 in the same preparation gave a similar rectification index (RI) in the MSNs of both control and aVMAT2cKO mice (respectively 1.03 and 1.09; Figure 2d), indicating that the level of AMPARs lacking GluA2 was not affected by

astrocytic VMAT2 depletion. Taken together, these findings show that the loss of astrocyte VMAT2 correlates with stronger PFC transmission to DMS MSNs.

Re-expression of VMAT2 in mPFC astrocytes rescues excessive grooming and anxiety-like behaviour

In order to determine the significance of astrocyte VMAT2 expression in OCD-relevant phenotypes, we evaluated the effects of mPFC astrocyte VMAT2 re-expression on the increased grooming and anxietylike behaviours observed in aVMAT2cKO mice. As shown in Figure 1, the aVMAT2cKO mice spent significantly more time grooming in the open field than control mice. A single intracranial injection of the astrocyte-specific lentiviral vector LentiVMAT2 (36, 45) at P25 (Figures 3a and 3b), which enables the selective re-expression of astrocyte VMAT2 (36) and normalized basal extracellular DA levels in the mPFC (36), reduced grooming activity of aVMAT2cKO mice (Figures 3c, 3d, 3e and 3f).

Furthermore, LentiVMAT2 treatment also increased the open field locomotion activities of the aVMAT2cKO mice (Figure 3g) and corrected the anxiety-like phenotype of the aVMAT2cKO mice (Figure 3h). We investigated the anxiolytic effects of VMAT2 further using the elevated plus maze test and we found that the LentiVMAT2 increased the time spent in the open arms of the maze (Figure 3i) and decreased the latency to enter in the distal part of the open arms (Figure 3j) of aVMAT2cKO mice. Control lentiviral injection (i.e. LentiGFP) had no significant effects on any measure of grooming and anxiety in the control mice, thus demonstrating that loss of VMAT2 in astrocytes contributes to the heightened pathological grooming and anxiety-like phenotypes of aVMAT2cKO mice.

We further examined whether the re-insertion of VMAT2 in mPFC astrocytes during postnatal development prevents the plasticity of the MSNs synapses of aVMAT2cKO mice (Figures 3k) by assessing the A/N ratio at mPFC to DMS synapses. Control lentiviral injection had no significant effect, but LentiVMAT2 injection significantly prevented the increase in the A/N ratio in aVMAT2cKO mice (Figure 3l).

Deletion of VMAT2 in PFC astrocytes is sufficient to induce excessive grooming and anxiety-like behaviour

In order to assess whether PFC aVMAT2 deletion was sufficient to induce OCD-like behavioural phenotypes, we specifically deleted astrocyte VMAT2 from the mPFC by injecting VMAT2^{fllox/fllox} mice with a Lentiviral vector (46) carrying Cre recombinase (LentiCre) on P20. Mice injected with LentiGFP were used as control mice (Figures 4a and 4b). A single injection of LentiCre on P20 induced phenotypes similar to those previously observed in aVMAT2cKO mice (36): i.e. decreased extracellular levels of DA in the PFC (Figure 4c), and increased spine density on P40 (Figures 4d-e), and increase in neuronal activity (Figure 4f-h). At behavioural level, LentiCre in the PFC robustly increased the grooming activities of VMAT2^{fllox/fllox} mice, which were significantly greater than those of the VMAT2^{fllox/fllox} mice injected with LentiGFP (Figures 4i-k). In comparison with the TAM-treated mice, we noticed a striking difference in the time spent grooming of LentiCre injected mice both for mice carrying deletion of VMAT2 and control mice (Fig 1f), thus suggesting that grooming behaviour is sensitive to the environmental stress factors (i.e. daily intraperitoneal injection with TAM or vehicle, direct effects of TAM, different time period etc) (47-49). Similar to the aVMATcKO mice, LentiCre injected mice showed an increased anxious behavior measured in the open field and elevated plus maze tests. The LentiCre injection reproduced the anxiety-like phenotype of reduced time in the centre of the open field (Fig. 4m) but not the decrease in the distance travelled (Figure 4l), significantly decreased the percentage of time spent in the open arms of the elevated plus maze (Figure 4n-o) and increased the latency to enter into the distal part of the open arm (Figure 4p).

Briefly, these experiments show that the specific astrocytic deletion of VMAT2 in the mPFC is sufficient to reproduce the core symptoms that characterise the OCD-like phenotype of aVMAT2cKO mice.

Chronic treatment with L-DOPA rescues excessive grooming and anxiety-like behaviour in aVMAT2cKO mice

In order to verify the potential effect of DA levels in the OCD-like behaviour of aVMATcKO mice, at first we performed series of experiment to confirm the presence of the determinants of DA uptake, storage and metabolism in tdTomato-positive astrocytes and the decrease of DA in the PFC in the

absence of aVMAT2 (36). The tdTomato astrocytes obtained from control mice showed significant levels of plasma membrane transporters organic cation transporter 3 and plasma membrane monoamine transporter (OCT3 and PMAT, respectively), of intracellular vesicular transporter VMAT2 and of metabolic enzyme monoamine oxidase B (MAOB) RNA but no significant signal for the essential enzyme for DA production, tyrosine hydroxylase (TH) (Figure 5a and Supplementary Figure 2a-d). Measurements of the tissue levels of DA in homogenates of PFC aVMATcKO mice showed a significant TAM-induced decrease from P25 (Figure 5b), as expected (36) and in vivo microdialysis confirmed a 33% reduction in extra-cellular DA levels in the PFC (Figure 5c and Supplementary Figure 2e). Furthermore, when we checked the effect of systemic administration of D-amphetamine (D-AMPH 7.5 mg/kg i.p.), which is known to induce the release of DA from intracellular storage by reversing its flux through plasma membrane transporters (50), we found that the extracellular DA levels were significantly less (-37.8%) in the aVMATcKO mice with respect to control mice (Figure 5c and Supplementary Figure 2e). Interestingly, this effect was reversed by blocking plasma membrane OCT3 and PMAT transporters using 100 μ M of the isocyanine compound decynium 22 (D22) (51) (-30.3%) (Figure 5c and Supplementary Figure 2e), thus confirming that aVMAT2 plays a role in the storage of DA in the PFC. We then excluded neuronal defects in the synthesis or release of DA by measuring the expression of TH (the rate-limiting enzyme in neuronal DA biosynthesis) and the OCT3 transporter by Western blotting (WB) (Supplementary Figure 2f) and quantifying the massive release of DA from neuronal projections induced by the local injection of high-dose K⁺ (Figure 5d) with in vivo microdialysis. Taken together, these findings indicate that astrocytes manage about 30% of PFC DA.

In order to evaluate whether restoring DA levels during the post-natal period of PFC maturation was effective in reducing the abnormal behaviour of aVMAT2cKO mice, their increased anxiety and pathological grooming were evaluated after chronic treatment with L-DOPA (20 mg/kg i.p.), which is known to increase DA levels in the PFC (36). Indeed, twenty consecutive days of L-DOPA treatment (from P20 to P40) significantly reduced both anxiety-like behaviour, compared to vehicle treatment (Figures 5e-g) and excessive grooming (Figure 5h-j).

Expression of VMAT2 and DA metabolic pathways in human astrocytes

In order to assess the potential translational relevance of our findings, we obtained human frontal brain cortex samples and used previously validated polyclonal antibodies against TH, VMAT2, catechol-o-methyl transferase (COMT) and MAOB (36) to check the expression of the bona fide proteins involved in the synthesis, storage and degradation of DA. In line with previous findings in human and rodent brain tissues (36), immunolabelling experiments did not detect any signal for TH but did reveal the presence of COMT, MAOB and VMAT2 in >80% of GFAP-positive cells (Supplementary Figure 3a). In particular, the VMAT2 signal was clearly recognisable in one of the four previously identified major morphological sub-classes of GFAP-immunoreactive cells of adult human frontal lobe (52): large, typically tortuous and highly branched protoplasmic astrocytes with primary processes, located in layers 2-6 (Figure 6a-c). Interestingly, the VMAT2 signal was virtually absent or weak in human and mouse GFAP-positive visual cortex cells (Supplementary Figure 3b) thus confirming the frontal cortex-specific expression of astrocyte VMAT2.

We then checked for the presence of DA in the VMAT2-expressing GFAP-positive cells using a previously validated DA polyclonal antibody (36) (Supplementary Figure 3c) and, in line with findings in rodents (Figures 5c-d), immunostaining showed the co-localisation of VMAT2 and DA in astrocytes located in all of the layers of human cortical brain tissue (Figure 6c), thus showing that astrocytes expressing VMAT2 and containing DA are also present in human cortex.

Discussion

Here, we provide evidence that VMAT2 is expressed in mammalian astrocytes (both human and rodent) located in the frontal cortical regions and that adult mice lacking VMAT2 in astrocytes of the PFC show pathological grooming behaviours and increased anxiety. This phenotype is potentially interesting because it may be related to the aetiology of human OCD spectrum disorders such as human trichotillomania, which is characterised by repetitive stereotypical hair-pulling from various sites and leads to noticeable hair loss (53). The excessive grooming of VMAT2-deficient mice has some similarities to that previously identified in mice models of OCD, such as synapse-associated protein 90/postsynaptic density protein 5-associated protein 3 (SAPAP3)- and SLIT and NTRK-like protein-5 (Slitrk5)- deficient mice (7, 9) with the syntactic complex grooming chain patterns that are superstereotyped due to the overly rigid sequential patterns of action that have been observed also in OCD and trichotillomania (54, 55). The pathological overgrooming in these mutant mice are linked with corticostriatal synaptic dysfunctions in a circuit which has been also implicated in patients with OCD (9, 56). Previous measurements of basal synaptic transmission in the PFC of mice carrying the deletion of astrocyte VMAT2 made by recording input/output (I/O) curves have shown that synaptic efficacy is significantly increases in the absence of astrocyte VMAT2, and that this is due to the lack of the tonic suppression of the excitatory transmission caused by DA acting on D2 receptors (36). We have now confirmed increased neuronal activity in the PFC and the concomitant appearance of abnormal grooming behaviour in mice in which astrocyte VMAT2 was specifically deleted in the medial PFC, thus supporting the possible involvement of the PFC in the generation of abnormal repetitive behaviour. Over the last few years, evidence obtained from OCD patients and mouse models of OCD has suggested that hyperactivity in prefrontal cortical regions (the PFC and the orbito frontal cortex) is involved in generating abnormal repetitive behaviours (7, 9, 37). In line with this hypothesis, it has been found that the use of repeated optogenetic stimulation of mOFC-striatal projections to simulate OFC hyperactivity leads to a progressive increase in grooming and the evoked firing rate (10). The findings of our study suggest that the hyperactivity of mPFC excitatory transmission may cause repetitive behaviour by

potentiating mPFC cortico-striatal connections. Our use of optogenetic projection targeting allowed us to assess mPFC cortico-striatal connections by measuring the ratio between post-synaptic AMPAR and NMDAR excitatory current amplitudes, and revealed an increase in the efficacy of synaptic transmission. Like its effect on excessive grooming behaviour, the re-insertion of VMAT2 in PFC astrocytes was sufficient to rescue this potentiation of synaptic transmission, thus suggesting that the abnormal repetitive behaviour may be associated with stronger mPFC-to-striatum transmission. Similar synaptic potentiation has been found in the orbitofrontal cortex-striatal connections of a mouse model of compulsion in which the compulsive optogenetic self-stimulation of DAergic neurons is associated with peak activity in the terminals of projections from the orbito-frontal cortex (57), thus suggesting that compulsive behaviour in general may be explained by the failure of the top-down inhibition of stimulus response associations attributed to the PFC (56, 58). It is worth noting that a large number of studies have demonstrated that compulsive grooming in mice can also be induced by genetic and circuit manipulations associated with striatal dysfunction (7, 9). In our study, we also found VMAT2 in some ST astrocytes (36), and a recent analysis of the tissue content of monoamines (including DA) in control aVMAT2cKO mice has shown a slight but significant decrease in total DA content of ~24% (data not shown), thus indicating that we cannot exclude the possibility that slightly decreased DA levels in the striatum of aVMAT2cKO mice may have some direct effects on striatal synaptic plasticity.

Immunohistochemical analyses of human and rodent cortical tissues show that VMAT2 is enriched in astrocytes of the frontal cortex but undetectable in astrocytes of the visual cortex, thus suggesting that astrocyte VMAT2 plays a functional role in frontal cortical regions, and in line with this hypothesis frontal cortical regions are part of the rodent grooming and OCD circuitries. Other proteins involved in the control of mice PFC DAergic metabolism by astrocytes included the expression of metabolic enzymes COMT and MAOB (36). Here we expand our knowledge about by showing that human astrocytes express high levels of MAOB and COMT, thus reinforcing the idea that, in the presence of low concentrations of high-affinity dopamine transporter (DAT), PFC seems to mainly depend on secondary mechanisms such as the COMT and MAO metabolic enzymes in order to clear released DA from extracellular space (59-62). The mechanism underlying the way in which astrocyte VMAT2, affects behaviour may depend on the role of this protein in regulating extra-cellular DA levels in concert

with MAOB and COMT (36) and indeed we found that both re-expression of astrocyte VMAT2 and systemic treatment with L-DOPA, two conditions that restore PFC DA levels (36), are sufficient to rescue abnormal grooming and anxiety behaviours in the aVMAT2cKO mice. This provides a causal link between the absence of VMAT2 in astrocytes, decreased DA levels and the onset of OCD-like behaviour, and supports the hypothesis that increasing DA levels in the PFC may be therapeutically beneficial to patients with OCD.

Taken together, our findings not only indicate a novel role of PFC astrocytes in regulating cortico-striatal synaptic strength through DA homeostasis, but also show a phenotype that has not been previously associated with a decrease in astrocyte VMAT2. VMAT2 is an integral membrane protein that is expressed by aminergic cells in order to transport monoamines (particularly neurotransmitters such as DA, norepinephrine, serotonin and histamine) out of the cytoplasm and into the lumen of intra-cellular vesicles, including synaptic vesicles (63). By changing cytosolic and intra-vesicular monoamine concentrations, the up- or down-regulation of VMAT2 is crucial in regulating their homeostasis. Full VMAT2 knockout is lethal, and mouse studies have established that VMAT2 plays a critical role in maintaining catecholamine and serotonin levels in the central nervous system, and ensuring the availability of monoamines for exocytotic release from neurons (64). Given its crucial importance in regulating amines, human VMAT2 variants are very rare, but some have been associated with schizophrenia (65) and others with protection against alcohol neurotoxicity (66). Pathogenic variants in the gene encoding VMAT2 (i.e. SLC18A2) have only recently been described (67-69), cause severe forms of brain DA-serotonin vesicular transport disease and a variety of symptoms such as hypotonia, parkinsonism, tremor, developmental disability, and depression. Whether SLC18A2 participates in the pathophysiology of OCD has never been investigated, but our findings indicate the existence of an OCDlike phenotype specifically caused by a knockout in this gene in astrocytes. The presence of VMAT2 in astrocytes has only recently been identified by means of transcriptome analysis and immunohistochemistry (36, 70, 71), and a novel mRNA splice variant of *Drosophila* VMAT (DVMATB) has been found in a small sub-set of the glial cells in the lamina of the fly's optic lobe, where it regulates the homeostasis of histamine (72). Consequently, the pathological conditions

associated with the modulation of this gene in astrocytes are still unknown and require further investigation.

METHODS

See Supplemental Methods for a detailed description of experimental methods, and see Key Resources Table for materials and suppliers.

Maintenance, breeding and genotyping has been performed as previously described (36). Tamoxifen treatment has been performed as previously described (36). Stereotaxic intracranial injections have been performed as previously described (36). Tissue preparation, immunohistochemistry and histology have been performed as previously described (36). Microdialysis has been performed as previously described (36). Dendritic spine density and spine morphology was assessed as previously described (36). Preparation and imaging of human samples have been performed as previously described (75).

Virus preparation

We used Mokola and VSV-G pseudotyped LV to selectively express transgenes in astrocytes as previously described (45, 46). The astrocyte-specific expression of these viruses have been extensively characterised in our previous studies (see Supp. Figs. S3f,g and S3d (36), and Supp. Fig. 7a,b, (33, 73, 74).

Acknowledgments and disclosures

This study was supported by grants from the Swiss National Foundation NCCR Switzerland “Synapsy” (51NF40-158776), “Transcure” (51NF6240-16) (to P.B.), Swiss National Science Foundation SNSF (310030_185363) (to P.B.) and Telethon Italy (GGP20037) (to P.B.).

FP, TZ and PB designed, performed and analysed experiments. AL, SM, CC, LP, AMP, BMB, EDOF, GD, FM performed and analysed experiments. ND designed and produced viral constructs. LM provided surgical human samples. BG and JPM contributed to the critical reading of the manuscript. LS and MM designed, performed and analysed electrophysiological experiments. PB and LS, wrote the manuscript. PB supervised the project and directed the experiments.

We thank Fulvio Magara (CNP, UNIL) for advices on behavioral experiments and analysis; we are grateful to Vigna Graphic Design for assistance in designing, developing, and reviewing graphics and artwork.

Part of the results of this study was published as a preprint on bioRxiv: bioRxiv preprint doi:

<https://doi.org/10.1101/2021.01.27.428434>

The authors report no biomedical financial interests or potential conflicts of interests.

References

1. Berridge KC, Aldridge JW (2000): Super-stereotypy I: enhancement of a complex movement sequence by systemic dopamine D1 agonists. *Synapse*. 37:194-204.
2. Berridge KC, Fentress JC, Parr H (1987): Natural syntax rules control action sequence of rats. *Behav Brain Res*. 23:59-68.
3. Graybiel AM, Rauch SL (2000): Toward a neurobiology of obsessive-compulsive disorder. *Neuron*. 28:343-347.
4. Kalueff AV, Stewart AM, Song C, Berridge KC, Graybiel AM, Fentress JC (2016): Neurobiology of rodent self-grooming and its value for translational neuroscience. *Nat Rev Neurosci*. 17:45-59.
5. Ahmari SE, Dougherty DD (2015): Dissecting Ocd Circuits: From Animal Models to Targeted Treatments. *Depress Anxiety*. 32:550-562.
6. Chen M, Wan Y, Ade K, Ting J, Feng G, Calakos N (2011): Sapap3 deletion anomalously activates short-term endocannabinoid-mediated synaptic plasticity. *J Neurosci*. 31:9563-9573.
7. Shmelkov SV, Hormigo A, Jing D, Proenca CC, Bath KG, Milde T, et al. (2010): Slitrk5 deficiency impairs corticostriatal circuitry and leads to obsessive-compulsive-like behaviors in mice. *Nat Med*. 16:598-602, 591p following 602.
8. Ting JT, Feng G (2011): Neurobiology of obsessive-compulsive disorder: insights into neural circuitry dysfunction through mouse genetics. *Curr Opin Neurobiol*. 21:842-848.
9. Welch JM, Lu J, Rodriguiz RM, Trotta NC, Peca J, Ding JD, et al. (2007): Cortico-striatal synaptic defects and OCD-like behaviours in Sapap3-mutant mice. *Nature*. 448:894-900.
10. Ahmari SE, Spellman T, Douglass NL, Kheirbek MA, Simpson HB, Deisseroth K, et al. (2013): Repeated cortico-striatal stimulation generates persistent OCD-like behavior. *Science*. 340:1234-1239.
11. Benzina N, Mallet L, Burguiere E, N'Diaye K, Pelissolo A (2016): Cognitive Dysfunction in Obsessive-Compulsive Disorder. *Curr Psychiatry Rep*. 18:80.
12. Gruner P, Pittenger C (2017): Cognitive inflexibility in Obsessive-Compulsive Disorder. *Neuroscience*. 345:243-255.
13. Hadjas LC, Luscher C, Simmler LD (2019): Aberrant habit formation in the Sapap3-knockout mouse model of obsessive-compulsive disorder. *Sci Rep*. 9:12061.
14. Manning EE, Dombrovski AY, Torregrossa MM, Ahmari SE (2019): Impaired instrumental reversal learning is associated with increased medial prefrontal cortex activity in Sapap3 knockout mouse model of compulsive behavior. *Neuropsychopharmacology*. 44:1494-1504.
15. van den Boom BJG, Mooij AH, Miseviciute I, Denys D, Willuhn I (2019): Behavioral flexibility in a mouse model for obsessive-compulsive disorder: Impaired Pavlovian reversal learning in SAPAP3 mutants. *Genes Brain Behav*. 18:e12557.
16. Goodman WK, McDougle CJ, Price LH, Riddle MA, Pauls DL, Leckman JF (1990): Beyond the serotonin hypothesis: a role for dopamine in some forms of obsessive compulsive disorder? *J Clin Psychiatry*. 51 Suppl:36-43; discussion 55-38.
17. Nikolaus S, Antke C, Beu M, Muller HW (2010): Cortical GABA, striatal dopamine and midbrain serotonin as the key players in compulsive and anxiety disorders--results from in vivo imaging studies. *Rev Neurosci*. 21:119-139.
18. Olver JS, O'Keefe G, Jones GR, Burrows GD, Tochon-Danguy HJ, Ackermann U, et al. (2010): Dopamine D(1) receptor binding in the anterior cingulate cortex of patients with obsessive-compulsive disorder. *Psychiatry Res*. 183:85-88.
19. Ducasse D, Boyer L, Michel P, Loundou A, Macgregor A, Micoulaud-Franchi JA, et al. (2014): D2 and D3 dopamine receptor affinity predicts effectiveness of antipsychotic drugs in obsessivecompulsive disorders: a metaregression analysis. *Psychopharmacology (Berl)*. 231:3765-3770.
20. Kofuji P, Araque A (2021): Astrocytes and Behavior. *Annu Rev Neurosci*. 44:49-67.
21. Oliveira JF, Sardinha VM, Guerra-Gomes S, Araque A, Sousa N (2015): Do stars govern our actions? Astrocyte involvement in rodent behavior. *Trends Neurosci*. 38:535-549.
22. Santello M, Toni N, Volterra A (2019): Astrocyte function from information processing to cognition and cognitive impairment. *Nat Neurosci*. 22:154-166.
23. Banasr M, Duman RS (2008): Glial loss in the prefrontal cortex is sufficient to induce

- depressive-like behaviors. *Biol Psychiatry*. 64:863-870.
24. Lima A, Sardinha VM, Oliveira AF, Reis M, Mota C, Silva MA, et al. (2014): Astrocyte pathology in the prefrontal cortex impairs the cognitive function of rats. *Mol Psychiatry*. 19:834-841.
 25. Araque A, Carmignoto G, Haydon PG, Oliet SH, Robitaille R, Volterra A (2014): Gliotransmitters travel in time and space. *Neuron*. 81:728-739.
 26. Araque A, Parpura V, Sanzgiri RP, Haydon PG (1999): Tripartite synapses: glia, the unacknowledged partner. *Trends Neurosci*. 22:208-215.
 27. Bezzi P, Volterra A (2011): Astrocytes: powering memory. *Cell*. 144:644-645.
 28. Perea G, Navarrete M, Araque A (2009): Tripartite synapses: astrocytes process and control synaptic information. *Trends Neurosci*. 32:421-431.
 29. Petrelli F, Bezzi P (2016): Novel insights into gliotransmitters. *Curr Opin Pharmacol*. 26:138-145.
 30. Santello M, Cali C, Bezzi P (2012): Gliotransmission and the tripartite synapse. *Adv Exp Med Biol*. 970:307-331.
 31. Petrelli F, Bezzi P (2018): mGlu5-mediated signalling in developing astrocyte and the pathogenesis of autism spectrum disorders. *Curr Opin Neurobiol*. 48:139-145.
 32. Petrelli F, Pucci L, Bezzi P (2016): Astrocytes and Microglia and Their Potential Link with Autism Spectrum Disorders. *Front Cell Neurosci*. 10:21.
 33. Zehnder T, Petrelli F, Romanos J, De Oliveira Figueiredo EC, Lewis TL, Jr., Deglon N, et al. (2021): Mitochondrial biogenesis in developing astrocytes regulates astrocyte maturation and synapse formation. *Cell Rep*. 35:108952.
 34. Aida T, Yoshida J, Nomura M, Tanimura A, Iino Y, Soma M, et al. (2015): Astroglial glutamate transporter deficiency increases synaptic excitability and leads to pathological repetitive behaviors in mice. *Neuropsychopharmacology*. 40:1569-1579.
 35. Yu X, Taylor AMW, Nagai J, Golshani P, Evans CJ, Coppola G, et al. (2018): Reducing Astrocyte Calcium Signaling In Vivo Alters Striatal Microcircuits and Causes Repetitive Behavior. *Neuron*. 99:1170-1187 e1179.
 36. Petrelli F, Dallerac G, Pucci L, Cali C, Zehnder T, Sultan S, et al. (2020): Dysfunction of homeostatic control of dopamine by astrocytes in the developing prefrontal cortex leads to cognitive impairments. *Mol Psychiatry*. 25:732-749.
 37. Ahmari SE, Rauch SL (2022): The prefrontal cortex and OCD. *Neuropsychopharmacology*. 47:211-224.
 38. Narboux-Neme N, Sagne C, Doly S, Diaz SL, Martin CB, Angenard G, et al. (2011): Severe serotonin depletion after conditional deletion of the vesicular monoamine transporter 2 gene in serotonin neurons: neural and behavioral consequences. *Neuropsychopharmacology*. 36:2538-2550.
 39. Hirrlinger PG, Scheller A, Braun C, Hirrlinger J, Kirchhoff F (2006): Temporal control of gene recombination in astrocytes by transgenic expression of the tamoxifen-inducible DNA recombinase variant CreERT2. *Glia*. 54:11-20.
 40. Prut L, Belzung C (2003): The open field as a paradigm to measure the effects of drugs on anxiety-like behaviors: a review. *Eur J Pharmacol*. 463:3-33.
 41. Monteiro P, Feng G (2016): Learning From Animal Models of Obsessive-Compulsive Disorder. *Biol Psychiatry*. 79:7-16.
 42. Zuchner S, Wendland JR, Ashley-Koch AE, Collins AL, Tran-Viet KN, Quinn K, et al. (2009): Multiple rare SAPAP3 missense variants in trichotillomania and OCD. *Mol Psychiatry*. 14:6-9.
 43. Piantadosi SC, Ahmari SE (2015): Using Optogenetics to Dissect the Neural Circuits Underlying OCD and Related Disorders. *Curr Treat Options Psychiatry*. 2:297-311.
 44. Klapoetke NC, Murata Y, Kim SS, Pulver SR, Birdsey-Benson A, Cho YK, et al. (2014): Independent optical excitation of distinct neural populations. *Nat Methods*. 11:338-346.
 45. Colin A, Faideau M, Dufour N, Auregan G, Hassig R, Andrieu T, et al. (2009): Engineered lentiviral vector targeting astrocytes in vivo. *Glia*. 57:667-679.
 46. Humbel M, Ramosaj M, Zimmer V, Regio S, Aeby L, Moser S, et al. (2021): Maximizing lentiviral vector gene transfer in the CNS. *Gene Ther*. 28:75-88.
 47. Fernandez-Teruel A, Estanislau C (2016): Meanings of self-grooming depend on an inverted Ushaped function with aversiveness. *Nat Rev Neurosci*. 17:591.

48. Geuther BQ, Peer A, He H, Sabnis G, Philip VM, Kumar V (2021): Action detection using a neural network elucidates the genetics of mouse grooming behavior. *Elife*. 10.
49. Li X, Du ZJ, Chen MQ, Chen JJ, Liang ZM, Ding XT, et al. (2020): The effects of tamoxifen on mouse behavior. *Genes Brain Behav*. 19:e12620.
50. Kahlig KM, Binda F, Khoshbouei H, Blakely RD, McMahon DG, Javitch JA, et al. (2005): Amphetamine induces dopamine efflux through a dopamine transporter channel. *Proc Natl Acad Sci U S A*. 102:3495-3500.
51. Cui M, Aras R, Christian WV, Rappold PM, Hatwar M, Panza J, et al. (2009): The organic cation transporter-3 is a pivotal modulator of neurodegeneration in the nigrostriatal dopaminergic pathway. *Proc Natl Acad Sci U S A*. 106:8043-8048.
52. Oberheim NA, Takano T, Han X, He W, Lin JH, Wang F, et al. (2009): Uniquely hominid features of adult human astrocytes. *J Neurosci*. 29:3276-3287.
53. Chamberlain SR, Odlaug BL, Boulougouris V, Fineberg NA, Grant JE (2009): Trichotillomania: neurobiology and treatment. *Neurosci Biobehav Rev*. 33:831-842.
54. Frances AJ PH, First B, Ross R, Davis W (2013): *Diagnostic and Statistical Manual of Mental Disorders*. 5th ed ed.: American Psychiatric Association.
55. Lamothe H, Baleyte JM, Mallet L, Pelissolo A (2020): Trichotillomania is more related to Tourette disorder than to obsessive-compulsive disorder. *Braz J Psychiatry*. 42:87-104.
56. Gillan CM, Robbins TW (2014): Goal-directed learning and obsessive-compulsive disorder. *Philos Trans R Soc Lond B Biol Sci*. 369.
57. Pascoli V, Hiver A, Van Zessen R, Loureiro M, Achargui R, Harada M, et al. (2018): Stochastic synaptic plasticity underlying compulsion in a model of addiction. *Nature*. 564:366-371.
58. Hadjas LC, Schartner MM, Cand J, Creed MC, Pascoli V, Luscher C, et al. (2020): Projection-specific deficits in synaptic transmission in adult Sapap3-knockout mice. *Neuropsychopharmacology*. 45:2020-2029.
59. Diamond A (2007): Consequences of variations in genes that affect dopamine in prefrontal cortex. *Cereb Cortex*. 17 Suppl 1:i161-170.
60. Kaenmaki M, Tammimaki A, Myohanen T, Pakarinen K, Amberg C, Karayiorgou M, et al. (2010): Quantitative role of COMT in dopamine clearance in the prefrontal cortex of freely moving mice. *J Neurochem*. 114:1745-1755.
61. Mazei MS, Pluto CP, Kirkbride B, Pehek EA (2002): Effects of catecholamine uptake blockers in the caudate-putamen and subregions of the medial prefrontal cortex of the rat. *Brain Res*. 936:58-67.
62. Mundorf ML, Joseph JD, Austin CM, Caron MG, Wightman RM (2001): Catecholamine release and uptake in the mouse prefrontal cortex. *J Neurochem*. 79:130-142.
63. Liu Y, Edwards RH (1997): The role of vesicular transport proteins in synaptic transmission and neural degeneration. *Annu Rev Neurosci*. 20:125-156.
64. Wang YM, Gainetdinov RR, Fumagalli F, Xu F, Jones SR, Bock CB, et al. (1997): Knockout of the vesicular monoamine transporter 2 gene results in neonatal death and supersensitivity to cocaine and amphetamine. *Neuron*. 19:1285-1296.
65. Chu TT, Liu Y (2010): An integrated genomic analysis of gene-function correlation on schizophrenia susceptibility genes. *J Hum Genet*. 55:285-292.
66. Lin Z, Walther D, Yu XY, Li S, Drgon T, Uhl GR (2005): SLC18A2 promoter haplotypes and identification of a novel protective factor against alcoholism. *Hum Mol Genet*. 14:1393-1404.
67. Jacobsen JC, Wilson C, Cunningham V, Glamuzina E, Prosser DO, Love DR, et al. (2016): Brain dopamine-serotonin vesicular transport disease presenting as a severe infantile hypotonic parkinsonian disorder. *J Inherit Metab Dis*. 39:305-308.
68. Rath M, Korenke GC, Najm J, Hoffmann GF, Hagendorff A, Strom TM, et al. (2017): Exome sequencing results in identification and treatment of brain dopamine-serotonin vesicular transport disease. *J Neurol Sci*. 379:296-297.
69. Rilstone JJ, Alkhater RA, Minassian BA (2013): Brain dopamine-serotonin vesicular transport disease and its treatment. *N Engl J Med*. 368:543-550.
70. Cahoy JD, Emery B, Kaushal A, Foo LC, Zamanian JL, Christopherson KS, et al. (2008): A transcriptome database for astrocytes, neurons, and oligodendrocytes: a new resource for understanding brain development and function. *J Neurosci*. 28:264-278.

71. Zhang Y, Chen K, Sloan SA, Bennett ML, Scholze AR, O'Keeffe S, et al. (2014): An RNAsequencing transcriptome and splicing database of glia, neurons, and vascular cells of the cerebral cortex. *J Neurosci.* 34:11929-11947.
72. Romero-Calderon R, Uhlenbrock G, Borycz J, Simon AF, Grygoruk A, Yee SK, et al. (2008): A glial variant of the vesicular monoamine transporter is required to store histamine in the *Drosophila* visual system. *PLoS Genet.* 4:e1000245.
73. Pannasch U, Freche D, Dallerac G, Ghezali G, Escartin C, Ezan P, et al. (2014): Connexin 30 sets synaptic strength by controlling astroglial synapse invasion. *Nat Neurosci.* 17:549-558.
74. Richetin K, Steullet P, Pachoud M, Perbet R, Parietti E, Maheswaran M, et al. (2020): Tau accumulation in astrocytes of the dentate gyrus induces neuronal dysfunction and memory deficits in Alzheimer's disease. *Nat Neurosci.* 23:1567-1579.
75. Prada I, Marchaland J, Podini P, Magrassi L, D'Alessandro R, Bezzi P, et al. (2011): REST/NRSF governs the expression of dense-core vesicle gliosecretion in astrocytes. *J Cell Biol.* 193:537-549.

Legends

Figure 1. Facial lesions, excessive grooming and anxiety-like behaviors in aVMAT2cKO mice

A-B) Open field. **A)** Total distance travelled by control LoxTAM and aVMAT2cKO mice during 10 minutes of free exploration, **B)** percentage of time in the centre of the arena, and * $p < 0.01$; **** $p < 0.0001$ (n=14 in each group; unpaired Student's t-test). **C-D)** Elevated plus maze. **C)** Latency to enter in the distal part of the open arms for LoxTAM and aVMAT2cKO mice and **D)** percentage of time that the control LoxTAM and aVMAT2cKO mice spent in the open arms. * $p < 0.01$; *** $p < 0.001$ (n=8 in each group unpaired Student's t-test). **E-H)** Repetitive behaviors. **E)** Time that control LoxTAM and aVMAT2cKO mice spent in grooming, digging and jumping in their home cages. The error bars indicate the SEM * $p < 0.005$ (n=14 mice in each group; unpaired Student's t-test). **F)** Percentage of time that the control LoxTAM and aVMAT2cKO mice spent in grooming in the open field test **** $p < 0.0001$ (n=14 in each group; unpaired Student's t-test). The error bars indicate the SEM. **G)** Grooming bouts of the control LoxTAM and aVMAT2cKO mice in the open field test **** $p < 0.0001$ (n=14 in each group; unpaired Student's t-test). The error bars indicate the SEM. **H)** Length of grooming bouts of the control LoxTAM and aVMAT2cKO mice in the open field test * $p < 0.01$ (n=14 in each group; unpaired Student's t-test). **I-K)** Representative pictures from an adult control LoxTAM and an aVMAT2cKO mouse. The latter displays hair loss from facial regions. **K)** Representative pictures of a control LoxTAM mouse with hair loss due to allogrooming by its aVMATcKO mouse cage mate.

Figure 2. Alterations in mPFC-to-DMS synapses of aVMAT2cKO mice.

A) Location of virus injection and infection. AAV8-Syn-ChrimsonR-GFP was injected into the mPFC of the control LoxTAM and aVMAT2cKO mice. Cell nuclei were stained with Hoechst (blue). **B)** Whole-cell patch clamp recordings of striatal slices. The terminals of the mPFC-to-dorsomedial striatum (DMS) projections were stimulated with orange light (593 nm), and the light-evoked currents were recorded in putative medium-size spiny neurons (MSNs). For illustrative purposes, a patch-clamped

MSN was filled with biocytin (pink in right-hand picture). **C**) Example traces of patch-clamp recordings from LoxTAM (grey) and aVMAT2cKO mice (green). Left: A/N (-70/+40 mV); top right: A/N (+40/+40 mV); bottom right: rectification index. **D**) A/N ratios at holding currents of -70/+40 mV (left panel; n (cells) = 18 LoxTAM, 19 aVMAT2cKO; Mann-Whitney test, * $p < 0.05$) and +40/+40 mV (middle panel; n (cells) = 17 LoxTAM, 20 aVMAT2cKO; unpaired t-test: * $p < 0.05$), were significantly increased in the aVMAT2cKO mice, but the rectification index (right panel) was not significantly different between genotypes (n (cells) = 18 LoxTAM, 20 aVMAT2cKO; Mann-Whitney test: $p = 0.89$). Data are mean \pm SEM.

Figure 3. Astrocytic VMAT2 re-expression in the mPFC rescues the behavioral deficits and synaptic alterations of aVMAT2cKO mice. **A**) Schematic representation of the control GFP virus (LentiGFP) or LentiVMAT2 virus injection in the mPFC (prelimbic/infralimbic). **B**) Left: representative confocal coronal image showing the infection in the mPFC. Scale bar = 500 μ m. Centre: high magnification confocal images of LentiGFP (green), DAPI (blue) and glutamine synthase (GS) (red) in the mPFC. Scale bar = 20 μ m. Right: event timeline of daily intra-peritoneal injections of tamoxifen (P20-P28) and local infection with LentiVMAT2 or LentiGFP (P25). Behavioral and patch-clamp experiment were conducted starting P40. **C-F**) Repetitive behaviors. **C**) Average time that control LoxTAM mice, aVMAT2cKO mice infected with LentiGFP virus and aVMAT2cKO mice infected with LentiVMAT2 virus spent in grooming and digging in their home cages. ** $p < 0.005$ (n=14 each group; one-way ANOVA, followed by Tukey's post hoc test) **D**) Percentage of time that the control LoxTAM and aVMAT2cKO mice infected with LentiGFP or LentiVMAT2 virus spent grooming in the open field. *** $p < 0.001$, **** $p < 0.0001$ (n=8-16; one-way ANOVA, followed by Tukey's post hoc HSD test). **E-F**) The graphs shows the grooming bouts and grooming length of control LoxTAM and aVMAT2cKO mice infected with LentiGFP or LentiVMAT2 virus *** $p < 0.001$ (n=8-16 each group; one-way ANOVA, followed by Tukey's post hoc HSD test). **G-H**) Open field. **G**) The histograms show the average total distance travelled by control LoxTAM and aVMAT2cKO mice infected with LentiGFP or LentiVMAT2 virus during 10 minutes of free exploration, and **H**) the average percentage of time the

spent in the center of the arena. * $p < 0.05$, ** $p < 0.005$, *** $p < 0.001$ (n=8-16 in each group, one-way ANOVA, followed by Tukey's post hoc HSD test). **I-J**) Elevated plus maze. The histograms show the latency to enter into the distal part of the open arm and average percentage of time spent in the open arms of control LoxTAM and aVMAT2cKO mice infected with LentiGFP virus or LentiVMAT2 virus. * $p < 0.01$, ** $p < 0.005$ (n=8-16; one-way ANOVA, followed by Tukey's post hoc HSD test) **K-L**) Ex vivo slice electrophysiology. **K**) Schematic of virus injection. **L**) The aVMAT2cKO mice injected with LentiGFP showed a significantly higher A/N ratio (measured at holding currents -70/+40 mV) compared to the LoxTAM + LentiGFP control group, but the selective re-expression of VMAT2 in the mPFC of aVMAT2cKO mice prevented the emergence of the synaptic phenotype (n (cells)= 15 LoxTAM + LentiGFP, 25 aVMAT2cKO + LentiGFP, 22 aVMAT2cKO + LentiVMAT2; one-way ANOVA: $P = 0.0009$, $F(2,59) = 7.948$; Tukey's post hoc test: * $p < 0.05$, *** $p < 0.001$). The error bars indicate SEM.

Figure 4. Deletion of VMAT2 in mPFC astrocytes is sufficient to cause OCD-like behavioral deficits. **A**) Schematic representation of Lentiviral vector carrying cre recombinase (LentiCre) or GFP (LentiGFP) injection in the mPFC (prelimbic/infralimbic). **B**) Representative high magnification confocal images of LentiCre (red) and GS (green) in the mPFC. Scale bar = 50 μm **C**) DA levels determined in extra-cellular perfusates of in vivo microdialysis in the PFC of control VMAT2_{flx/flx} mice infected with LentiGFP and VMAT2_{flx/flx} mice infected with LentiCre virus, expressed as percentage of baseline levels. ** $p < 0.01$ (n=5 each group, unpaired Student's t-test). **D**) Spine density calculated in layer V of the PFC of control LoxTAM-ThyEGFP mice and VMAT2_{flx/flx}-ThyEGFP mice infected with LentiCre virus. ** $p < 0.01$ (n=16 each group, unpaired Student's t-test). **E**) Representative confocal images showing Layer V mPFC dendritic spines in control LoxTAM-ThyEGFP mice and VMAT2_{flx/flx}-ThyEGFP mice infected with LentiCre virus. **F-H**) VMAT2 deletion in astrocytes increase action potential firing evoked by extracellular stimulation. **F**) Sample traces of current-clamp recordings ($I = 0$) from a Layer 5 pyramidal neuron recorded from a Lenti-GFP infused side and another neuron recorded in the contralateral hemisphere with Lenti-Cre. In the presence of DL-AP5 (100 μM), picrotoxin (100 μM), and SCH-50911 (20 μM), a train of five stimuli (20 Hz) induced EPSPs

that triggered action potentials. **G)** Box-plots and scatter-plot representing the number of action potentials per sweep in all experimental conditions (n mice=3, n cells=11-14, t-test $t_{23}=2.6$, $*p=0.0168$). **H)** Cumulative probability for the experimental data set. Bars represent the mean \pm SEM. **I-O)** Repetitive behaviors. **I)** Time that control VMAT2^{fllox/fllox} mice infected with LentiGFP and VMAT2^{fllox/fllox} mice infected with LentiCre virus spent grooming, digging and jumping in their home cages. $*p<0.05$ (n=5 each group, unpaired Student's t-test). The error bars indicate the SEM. **J-K)** Grooming bouts and bouts length in the open field of VMAT2^{fllox/fllox} mice infected with LentiGFP and VMAT2^{fllox/fllox} mice infected with LentiCre virus. $*p<0.05$ (n=5 each group, unpaired Student's t-test). **L-M)** Open field. **L)** Total distance travelled by VMAT2^{fllox/fllox} mice infected with LentiGFP and VMAT2^{fllox/fllox} mice infected with LentiCre virus during 10 minutes of free exploration (n=5 each group, unpaired Student's t-test), and **M)** percentage of time they spent in the centre of the arena. $*p<0.05$ (n=5 each group, unpaired Student's t-test). **N-P)** Elevated plus maze. **N)** Percentage of time spent in the open arms, **O)** time spent in the distal part of the open arms and **P)** the latency to enter into the distal part of the open arm of VMAT2^{fllox/fllox} mice infected with LentiGFP and VMAT2^{fllox/fllox} mice infected with LentiCre virus. $*p<0.05$ (n=5 each group, unpaired Student's t-test). The error bars indicate the SEM.

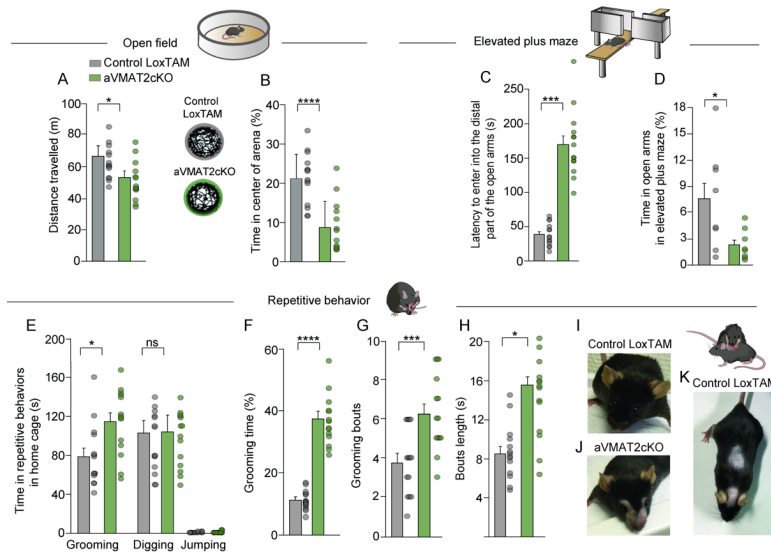
Figure 5. Deletion of VMAT2 in astrocytes decreases DA levels that seems to be crucial in inducing OCD-like behavior

A) Representative image of semi-quantitative PCR analysis of mRNA levels for VMAT2, OCT3, PMAT, MAOB and TH measured in FACS sorted astrocytes from control CreERT2XR26-tdTomato mice. (n=3 mice) **B)** Total DA content in PFC homogenates. Consistent with VMAT2 ablation, five days after TAM treatment DA (P25) was reduced by $35.4 \pm 4.7\%$ in the recombined aVMAT2cKO PFC tissue homogenates in comparison with those of the control LoxTAM mice. $*p<0.05$ (n=3 mice each group, Student's t test). **C)** DA levels determined in extra-cellular perfusates of the in vivo microdialysis in the PFC of recombined aVMAT2cKO and control LoxTAM mice treated with vehicle (saline solution 0.9% i.p.), D-amphetamine (D-AMPH, 7.5 mg/kg i.p.), or D-AMPH in the presence of D-22 (100 μ M local perfusion). The microdialysis probes were placed in the PFC, and DA levels (pg/ μ l) were measured at

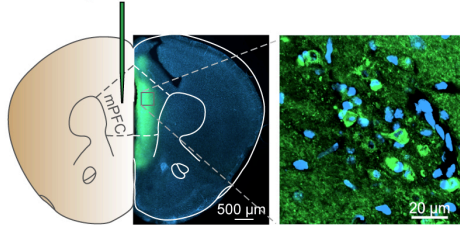
baseline for 30 min. ****p<0.001, *p<0.05** (n=6 mice, Student's t test). **D**) Curves show the average extracellular DA levels before and after the local injection of high K⁺ (100 mM) in the presence of in the presence of D-22 (100 μM local perfusion). Note that the release of DA induced by K⁺ in aVMAT2cKO is similar to control LoxTAM mice. (n=3). **E**) Open field. Percentage of time they spent in the centre of the arena. ****p<0.01** (n=8-11, one-way ANOVA, followed by Tukey's post hoc HSD test). **F-G**) Elevated plus maze. **F**) Percentage of time spent in the open arms and **G**) latency to enter into the distal part of the open arm of control LoxTAM, aVMAT2cKO and aVMAT2cKO mice chronically treated with L-DOPA/benserazide (20 mg/kg + 12.5 mg/kg) ****p<0.005** (n=8-11; one-way ANOVA, followed by Tukey's post hoc HSD test). **H-J**) Repetitive behaviours. **H**) Average time that control LoxTAM mice, aVMAT2cKO and aVMAT2cKO mice chronically treated with LDOPA/ benserazide (20 mg/kg + 12.5 mg/kg) spent grooming and digging in their home cages. ****p<0.005** (n=10-14 each group; one-way ANOVA, followed by Tukey's post hoc HSD test). The error bars indicate the SEM. **I-J**) Grooming bouts and bouts length in the open field of control LoxTAM mice, aVMAT2cKO and aVMAT2cKO mice chronically treated with L-DOPA/benserazide (20 mg/kg + 12.5 mg/kg) ***p<0.05, **p<0.005** (n=8-11 each group; one-way ANOVA, followed by Tukey's post hoc HSD test).

Figure 6. VMAT2 and DA labeling in astrocytes of the human brain frontal cortex. All images (representative of six slices from two tissue samples) are z projections of stacks 8-μm thick. **A-B**) The VMAT2 immunolabeling (red) in the cell bodies and processes of astrocytes identified by the cytoplasmic marker GFAP (green). Some astrocytes exhibit high VMAT2 labeling of the soma (arrowheads, high magnification in a), whereas in others, VMAT2 is mainly expressed on processes (arrowheads, high magnification in b). Bar, 30 μm. **C**) The expression of VMAT2 (red) and DA (green) in the cell bodies and processes of astrocytes identified by the cytoplasmic marker GFAP. Bar, 30 μm.

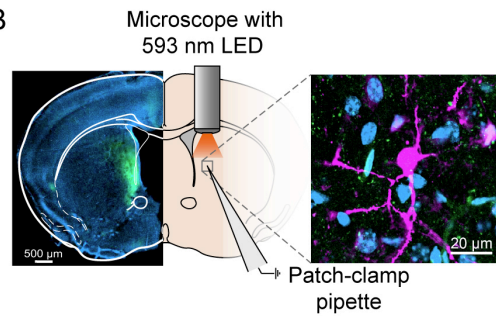
Figure 1



A AAV8-Syn-ChrimsonR-GFP

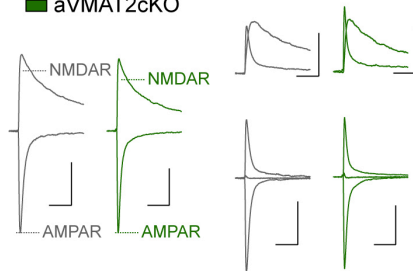


B

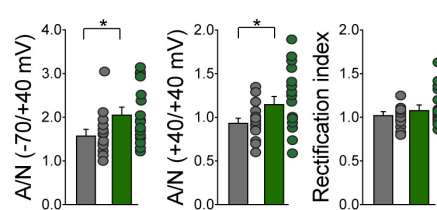


Control LoxTAM
aVMAT2cKO

C



D



Astrocyte-specific Lenti-GFP/VMAT2

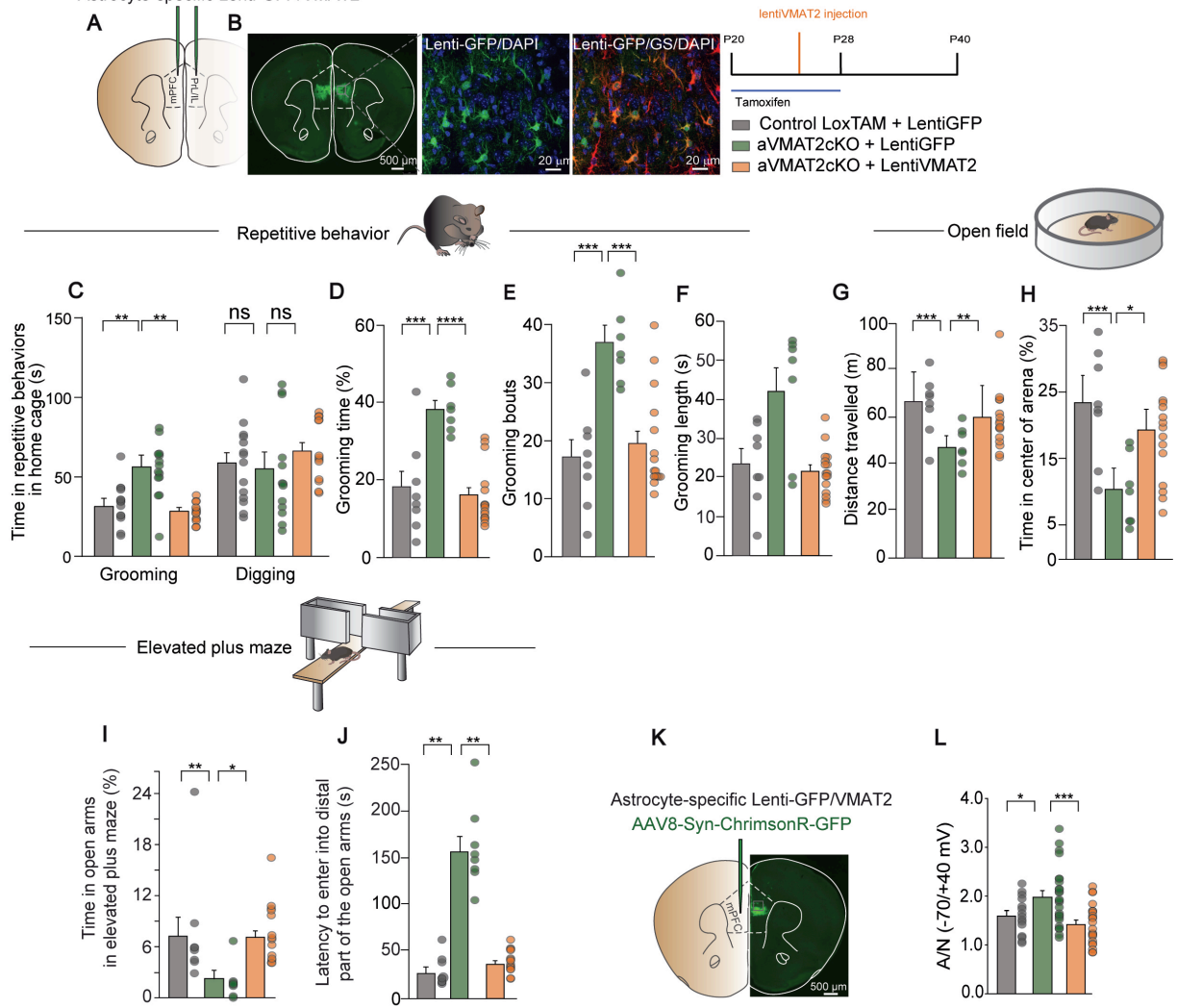
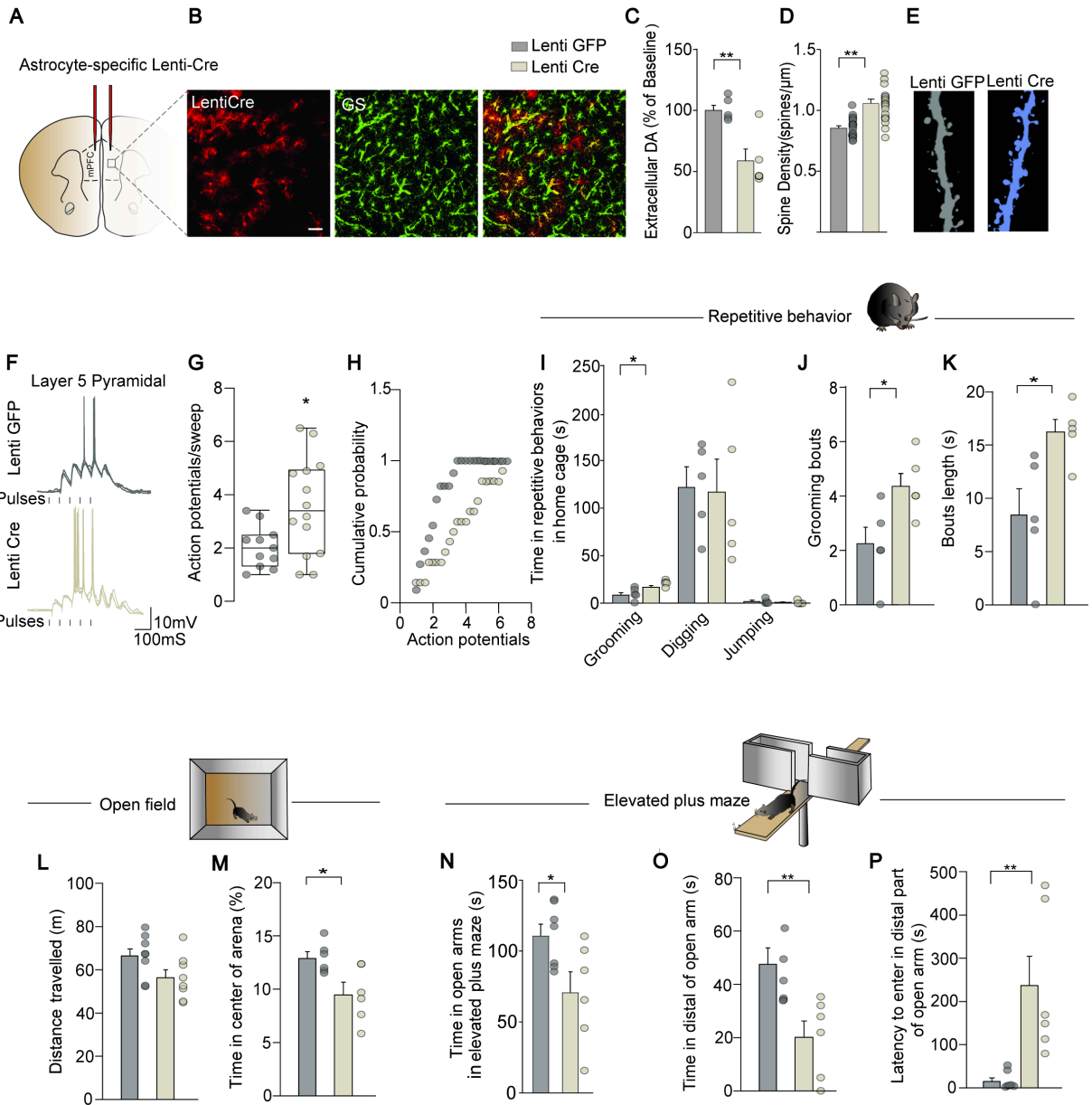


Figure 4



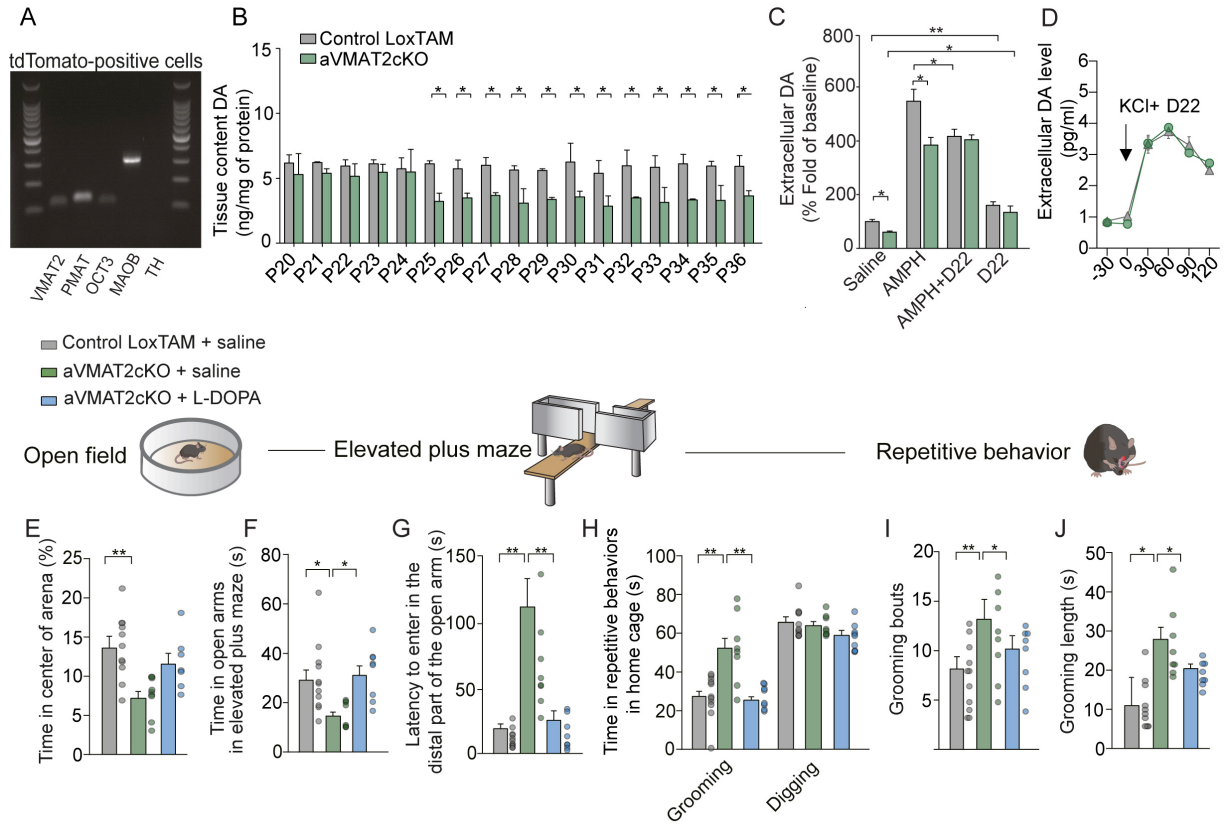


Figure 6

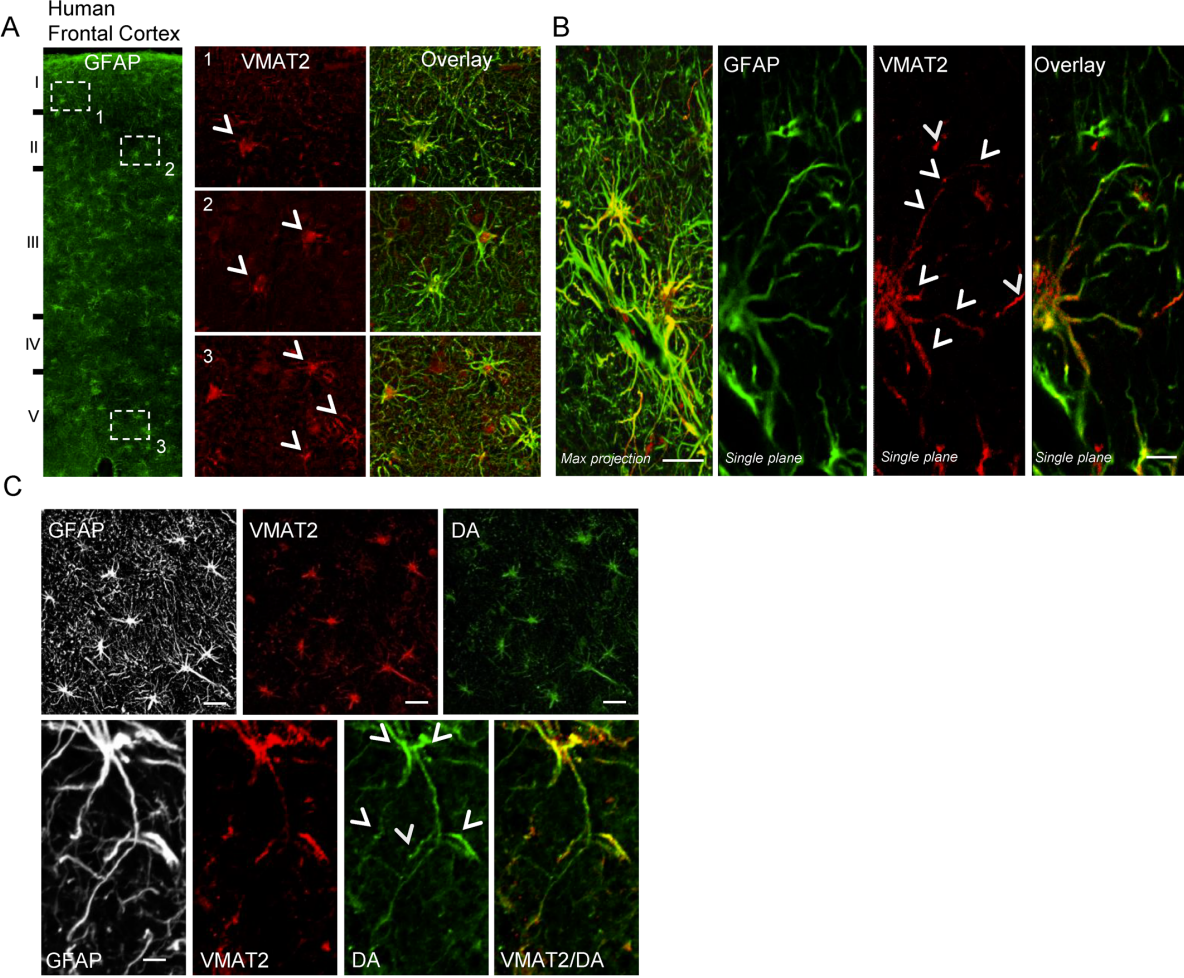
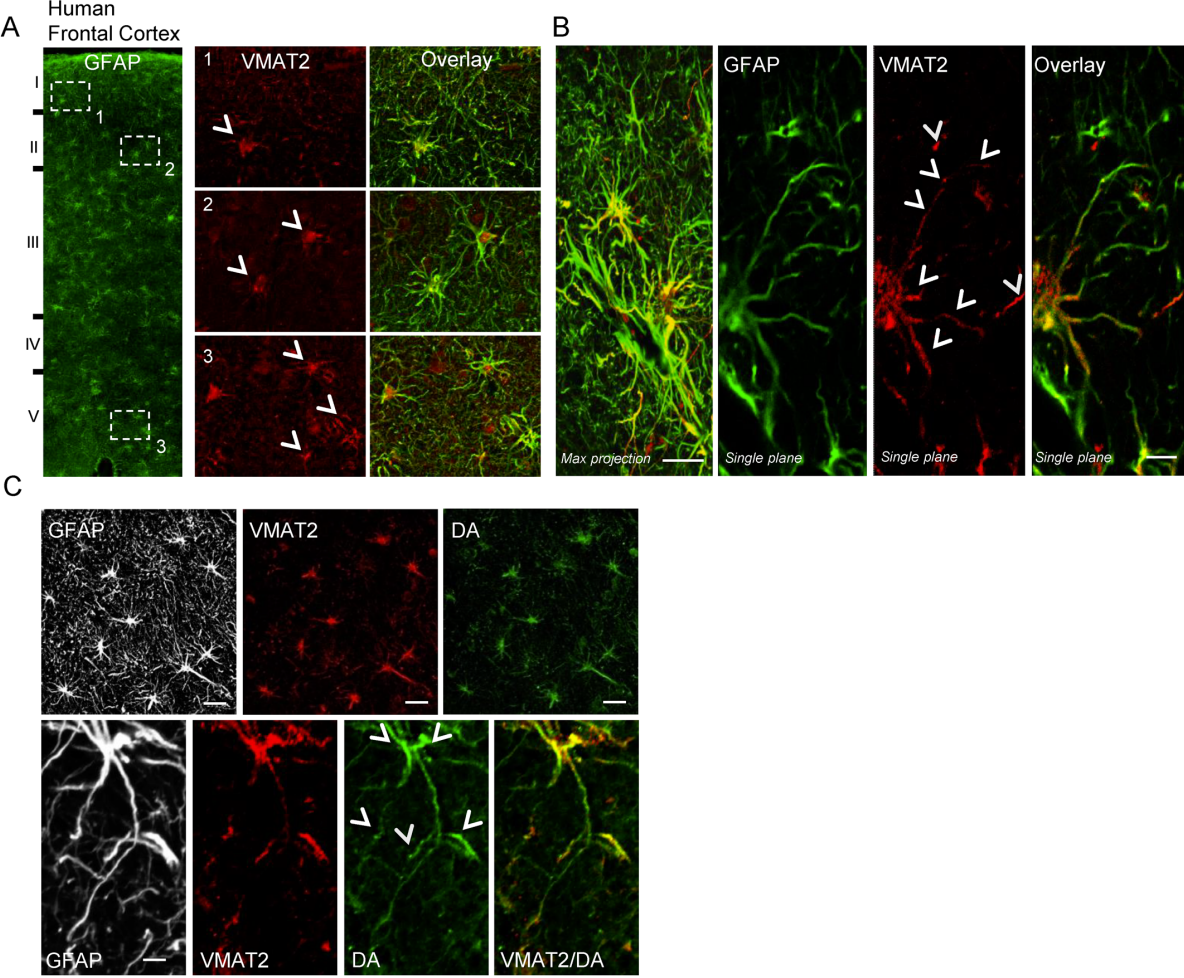


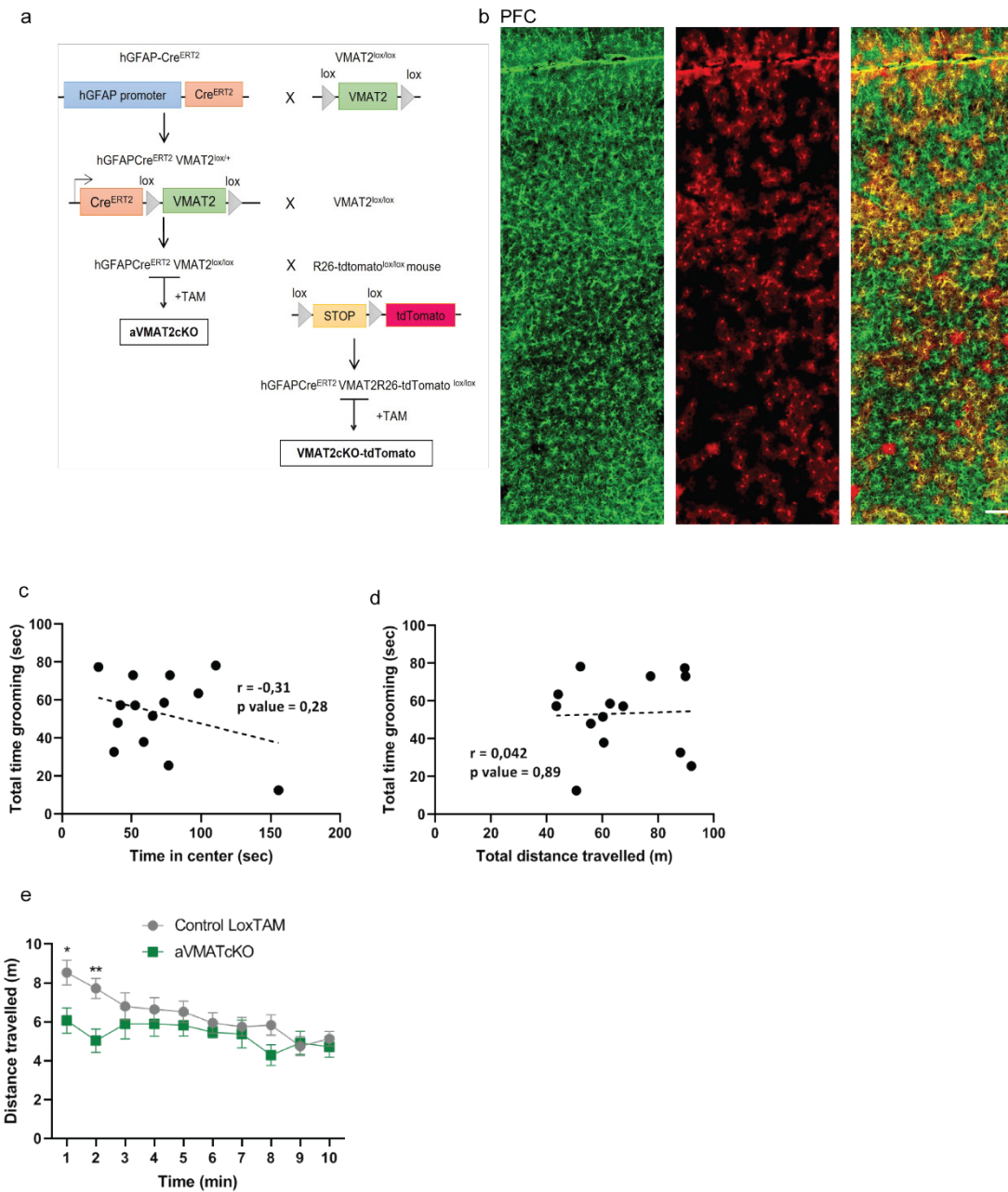
Figure 6



SUPPLEMENTARY INFORMATION

Disruption of Astrocyte-Dependent Dopamine Control in the Developing Medial Prefrontal Cortex Leads to Excessive Grooming in Mice

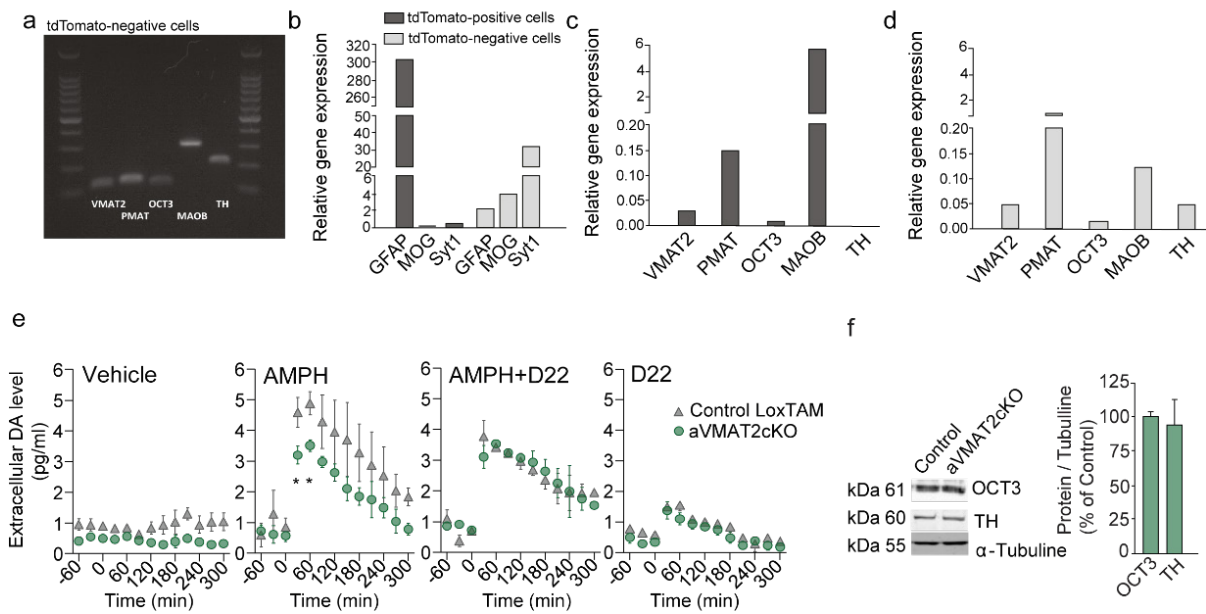
Petrelli *et al.*



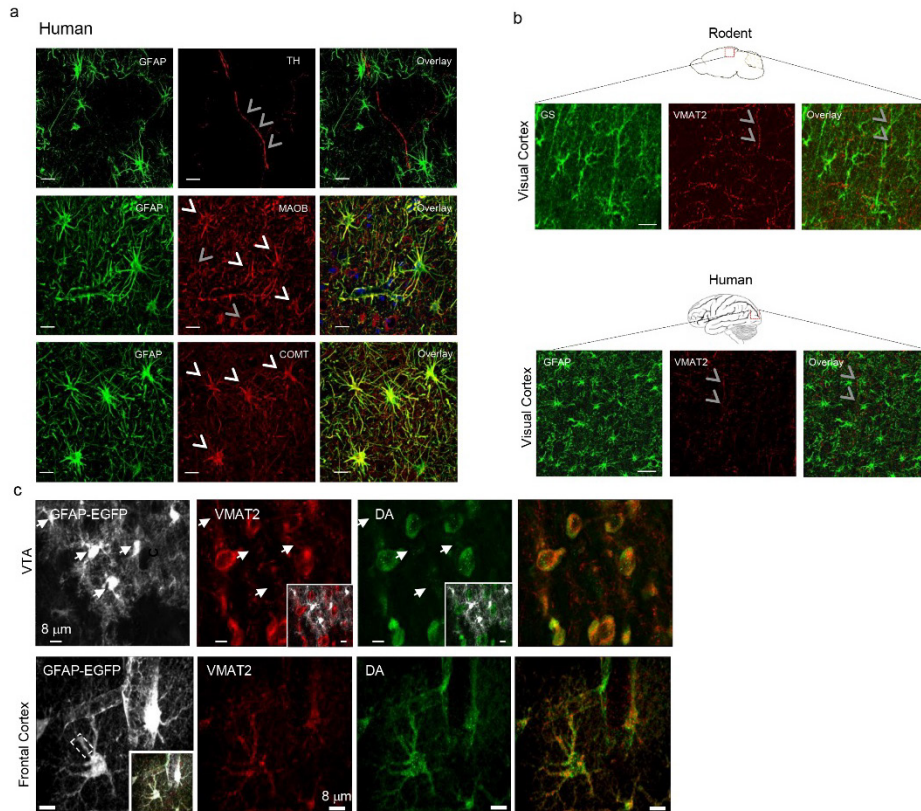
Supplementary Figure 1. Production and characterization of aVMAT2cKO mice

a) Schematic diagram of the generation of aVMAT2cKO mice showing that inducible knock-out mice in which astrocyte VMAT2 was specifically deleted in a temporally controlled manner were generated by cross breeding mice carrying an inducible form of Cre recombinase (Cre^{ERT2}) under the promoter of human GFAP (hGFAP) with mice carrying LoxP-flanked VMAT2 allele ($VMAT2^{lox/lox}$). The resulting $hGFAPCre^{ERT2}VMAT2^{lox/+}$ mice were cross-bred with $VMAT2^{lox/lox}$ mice and their progeny, $hGFAPCre^{ERT2}VMAT2^{lox/lox}$, was treated with TAM from P20 to P28. Part of the $hGFAPCre^{ERT2}VMAT2^{lox/lox}$ mice have been used to check the cell-type specificity of VMAT2 gene deletion in astrocytes by crossing them with R26-tdTomato^{lox/lox} mice that harbour a tamoxifen (TAM)-inducible fluorescent reporter tdTomato transgene driven by the human astrocytic glial fibrillary acidic

protein (hGFAP) promoter. The resulting mice, hGFAPCre^{ERT2}VMAT2R26-tdTomato^{lox/lox} mice, were treated with TAM obtaining VMAT2cKO-tdTomato mice. **b)** Confocal sections show TAM-induced tdTomato expression in the prefrontal cortex (PFC) of VMAT2cKO-tdTomato mice on P40. tdTomato fluorescence (red) is confined to glutamine synthase (GS)-positive astrocytes (green) in the PFC. Scale bar: 100 μ m. **c)** Correlation plot between time spent in the center of the open field and time spent grooming in the open field. n = 14; Pearson r = -0.31 p = 0.28. **d)** Correlation plot between total distance travelled and time spent grooming in the open field n = 14; Pearson r = 0.042 p = 0.89. **e)** Minute-by-minute analysis of distance travelled in the open field; repeated measures two-way ANOVA (genotype p = 0.111; time p = 0.0006; genotype \times time interaction p = 0.0054) followed by Fisher LSD test; * p<0.05 and **p<0.01.



Supplementary Figure 2 (referred to the main figure 5). Additional data on the quantification of mRNA levels of DAergic determinants in astrocytes and on DA extracellular levels a) Representative image of semi-quantitative PCR analysis of mRNA levels for VMAT2, OCT3, PMAT, MAOB and TH measured in FACS sorted tdTomato-negative cells from control Cre^{ERT2}XR26-tdTomato mice. **b)** qPCR analysis of the relative expression of GFAP, MOG and Syt1 mRNA in tdTomato-positive and tdTomato-negative FACS sorted cells relative to β -actin. **c-d)** qPCR analysis of the relative expression of VMAT2, OCT3, PMAT MAOB and TH mRNA in tdTomato-positive FACS-sorted astrocytes **c)** and in tdTomato-negative cells **d)** relative to β -actin. **e)** Curves show the time course average levels of DA determined in extra-cellular perfusates of the *in vivo* microdialysis in the PFC of recombined aVMAT2cKO and control LoxTAM mice treated with vehicle, D-amphetamine (D-AMPH, 7.5 mg i.p. per kg body weigh), or D-AMPH in the presence of D-22 (100 μ M local perfusion). The microdialysis probes were placed in the PFC, and DA levels (pg/ μ l) were measured at baseline for 30 min. * $p < 0.05$ (n=3, unpaired Student's t-test). The error bars indicate the SEM. **f)** Western blot analysis of OCT3 and TH expression in PFC tissues from P38. Left: representative western blot from aVMAT2cKO and control LoxTAM mice. Right: Quantification of OCT3 and TH expression in aVMAT2cKO mice expressed as a percentage of that of control LoxVMAT2. The data are normalised to tubulin. The error bars indicate the SEM.



Supplementary Figure 3 (referred to main figure 6). Characterization of human DAergic astrocytes. All images (representative of six slices from two tissue samples) are z projections of stacks 8- μ m thick. **a)** TH, MAOB and COMT immunolabeling (red) in the cell bodies and processes of astrocytes identified by the cytoplasmic marker GFAP (green). Note that human astrocytes exhibit MAOB and COMT labeling, but no significant signal for TH. Bar, 30 μ m. **b)** VMAT2 immunolabeling in the visual cortex of mouse and human tissue is localized in neuronal axons and not in GS or GFAP-expressing cells, respectively. Bar, 30 and 60 μ m, respectively **c)** VMAT2 and DA immunolabeling co-localizes in dopaminergic neurons of the VTA and in GFAP-EGFP astrocytes in the frontal cortex. Bar, 8 μ m

Supplementary Methods

Maintenance, breeding and genotyping

The animal studies were approved by the *Service de la consommation et des affaires vétérinaires du Canton Vaud* or the Institutional Animal Care and Use Committee of the University of Geneva and the animal welfare committee of the Canton of Geneva, in accordance with Swiss law. The mice were group-housed with littermates in standard housing with a 12:12-hour light:dark cycle. The hGFAPcre^{ERT2} mice (1) and ROSA26- tdTomato-hGFAPcre^{ERT2} mice (1, 2) were obtained from Frank Kirchhoff (Molecular Physiology, University of Saarland, Germany), the VMAT2^{lox/lox} mice (3) from Bruno Giros (Douglas Mental Health University Institute, Canada), and the tdTomato^{lox/lox} mice (AI14, Jackson Lab) and Thy1-EGFP mice from Joshua R. Sanes (Harvard University, USA). The mice used had a C57BL/6 background.

The hGFAPcre^{ERT2} sequence was identified from phalange biopsies using the following primers: 5'-CAGGTTGGAGAGGAGACGCATCA-3', 5'-CGTTGCATCGACCGGTAATGCAGGC-3'. The VMAT2^{lox/lox} sequence was identified using the following primers: 5'-GACTAGGGACAGCACAAATCTCC-3', 5'-GAAACATGAAGGACAACCTGGGACCC-3'. The ROSA26-EYFP sequence was identified using the following primers: 5'-AAAGTCGCTCTGAGTTGTTAT-3', 5'-GCGAAGAGTTTGTCTCAACC-3', 5'-GGAGCGGGAGAAATGGATATG-3.

The PCR reaction product coupled with Syber green migrated in a 1.5% agarose gel, and the bands were revealed by UV light.

Virus preparation

We used Mokola and VSV-G pseudotyped LV to selectively express transgenes in astrocytes. In both LentiVMAT2 and LentiCre, we used the recently described microRNA (miRNA) regulation pathway to develop mokola- or VSV-G-pseudotyped lentiviral vectors specifically targeting astroglial cells. We combined the mokola or VSV-G lentiviral vectors with the insertion of glutamine synthase (GS) or GfaABC1D(B)3 (G1B3) promoters for astrocytes and the miR124+miR9 target sequence in order to eliminate residual expression in neuronal cells and obtain restricted transgene expression in the astrocytes of different brain regions of adult mice (4, 5). The astrocyte-specific expression of these viruses have been extensively characterised in our previous studies (see Supp. Figs. S3f,g and S3d (6), and Supp. Fig. 7a,b, (7-9).

Stereotaxic intracranial injections

P25 mice were anaesthetised using isoflurane at 5% (w/v), placed in a small animal stereotaxic frame (David Kopf Instruments), and maintained at 2.5% isoflurane (w/c) for the duration of surgery. Corneal and pinch reflexes were regularly tested in order to confirm the depth of the anaesthesia. Lacryvisc (Aicon, Switzerland) was used to prevent corneal drying, and lidocaine was topically applied to the skin overlying the skull. After exposing the skull under aseptic conditions, a small hole was drilled into the skull overlying the prefrontal cortex (AP + 2.0 mm, L \pm 0.2 mm and DV -2.0 mm). LentiVMAT2, LentiCre and/or LentiGFP were injected (1 μ l total volume) bilaterally through a Hamilton syringe at a rate of 100 nl min⁻¹ using a CMA400 Pump (CMA System). Adeno-associated virus AAV8-hSyn-Chrimson-GFP (0.4 μ L each hemisphere; Duke University, Durham, USA) was injected at P30 into control LoxTAM and aVMAT2cKO mice bilaterally using a thin glass pipette connected to an injection wheel. After the surgical procedures, the mice were returned to their home cages for at least two weeks in order to allow maximum gene expression.

Tissue preparation, immunohistochemistry and histology

The mice were deeply anaesthetised using intraperitoneal sodium pentobarbitone (6 mg/100g body weight) and immediately perfused intracardially with fresh 4% paraformaldehyde in 0.1 M phosphate-buffered saline (PBS, pH 7.4). Their brains were post-fixed overnight, equilibrated in 30% sucrose at -20 °C using a cryostat (Leica), and stored at -80 °C. 50 μ m brain sections were permeabilised for 45 minutes in phosphate-buffered saline containing 0.3% Triton X-100, and 15% donkey or goat serum, and then immunolabelled overnight at 4 °C using the following primary antibodies: mouse-GS (Chemicon, 1:1000) (10), rabbit-GFP (Chemicon, 1:200) (11), rabbit-GFAP (Chemicon, 1:1000), rabbit-OCT3 (Alpha Diagnostics, 1:100), mouse-dopamine (Millipore, 1/100), rabbit-dopamine (Millipore, 1/1500), mouse-COMT (BD-Transduction Lab, 1/1000) goat-MAOB (Santa Cruz, 1:100), rabbit-VMAT2 (Synaptic System, 1:5600; Chemicon, 1:1000), and rabbit-TH (Millipore, 1:1000). The day after incubation with primary antibodies, the brain sections were washed three times in PBS for 10 minutes and then incubated for 1.5 hours at room temperature with fluorescent secondary antibodies (AlexaFluor, Invitrogen Molecular Probes, Eugene, Oregon, USA: goat anti-mouse 488, 555, and 633; goat anti-rabbit 488, 555, and 633; and donkey anti goat 488; 1:300 and 1:400) diluted in PBS. Finally, the nuclei were counterstained with 4', 6-diamidino-2-phenylindole (DAPI) (Invitrogen, 1:10000) and then washed before mounting with FluorSave (Calbiochem).

Preparation and imaging of human samples

The brain was extracted and washed in PBS. Fragments of normal structure from human brain temporal cortices were removed as part of the planned margin of resection surrounding a neoplastic lesion from patients operated at the Section of Neurosurgery in the Policlinic San Matteo. Surgery was performed according to the recommendations of the Institutional Review Boards and in full agreement with the

Declaration of Helsinki. Samples were fixed in 4% formaldehyde for 24 h and then washed in PBS. Human subject samples from informed and consenting human patients were collected before 2011 as previously described (12). All images were collected on a Leica confocal imaging system (TCS SP5) with a 40x (1.4 NA) or 63x (1.4 NA) oil immersion objective. Sections were acquired every 0.4 μm , and the confocal images were analysed using Imaris 7.6.3 (Bitplane AG, Zurich, Switzerland) or Adobe Photoshop CS5 software (Adobe System Inc., San José, California, USA).

***In vivo* microdialysis**

The mice were anaesthetised with isoflurane and placed in a stereotaxic frame using a mouse adaptor (David Kopf Instruments) with modified ear bars. Microdialysis probes were implanted in the PFC at the following coordinates relative to the bregma: AP +2.0 mm, ML +0.5 mm and DV –3.0 mm, with the tooth-bar set at 0 mm. The active dialysis surface length of the membrane was 2 mm. The probe was secured in place using dental cement on the skull.

The microdialysis experiments started 24 hours after surgery. Ringer solution (125 mM NaCl, 2.5 mM KCl, 1.26 mM CaCl₂, 1.18 mM MgCl₂, 0.20 mM NaH₂PO₄) was perfused through the microdialysis probe at a flow rate of 1.0 $\mu\text{l}/\text{min}$ using a high precision pump (CMA 400 syringe pump, CMA Sweden) (6). The experiments were performed during the light period of the light/dark cycle, and the mice were tested in their home cages. After an equilibration period of at least two hours, the dialysates were collected into small Eppendorf tubes containing 11.7 μL of acetic acid every 30 minutes, and stored at –69°C until high-performance liquid chromatography (HPLC) analysis. Dopamine levels were quantified by means of HPLC with electrochemical detection as previously described (6) with some modifications. The samples were injected into an MD-150 column (3 M, 3.2x150 mm, Thermo Fisher Scientific,) using a Thermo Scientific Dionex Ultimate 3000, and dopamine was detected at 32 °C using an ECD-3000RS electrochemical detector (Thermo Fisher Scientific) set at a potential of 250 mV against an Ag/AgCl reference electrode. The signal was analysed using Cromeleon, software. The mobile phase was 75 mM sodium dihydrogen phosphate monohydrate, 1.7 mM octane sulphonic acid sodium, 100 M triethylamine (TEA), 25 M EDTA, 10% acetonitrile, pH 3.00 with phosphoric acid. The flow rate was 0.5 mL/min.

Morphological analysis of dendrites and spines

Dendritic spine density and spine morphology was assessed as previously described (6). The spine analysis was made using two fluorescent transgenic mice strains: control LoxTAM-Thy1EGFP and VMAT2^{flx/flx}-Thy1EGFP mice obtained by crossbreeding Thy1EGFP with VMAT2^{flx/flx} mice. Confocal microscopy of post-fixed slices was performed using a Leica confocal imaging system (TCS SP5) with a 40 \times (1.8 NA) or 63x (2.8 NA) oil immersion objective. The mPFC field between Bregma coordinates 2.34 mm and 1.7 mm was analysed, with 50 μm brain sections being acquired every 0.4 μm .

The number of spines on 10-20 neurons per mouse was counted using image J software, and spine density was expressed as the number of spines divided by dendritic length (13).

Patch-clamp recordings

The mice were anaesthetised with isoflurane (5%) and decapitated, and their brains were quickly removed. Brain slices (220 μm thick) were cut using a vibratome in ice-cold oxygenated artificial cerebrospinal fluid (aCSF) containing NaCl 119 mM, D-glucose 11 mM, NaHCO_3 26.2 mM, KCl 2.5 mM, MgCl_2 1.3 mM, NaH_2PO_4 1 mM, and CaCl_2 2.5 mM. The slices were re-covered in aCSF at 30 °C for 15 minutes, and then kept at room temperature until use. The recordings were made in aCSF with 100 μM picrotoxin at 30 °C. The internal solution consisted of 130 mM CsCl, 4 mM NaCl, 5 mM creatine phosphate, 2 mM MgCl_2 , 2 mM Na_2ATP , 0.6 mM Na_3GTP , 1.1 mM EGTA, 5 mM HEPES, 5 mM QX-314, and 0.1 mM spermine. The currents were amplified using Multiclamp 700B (Axon Instruments), filtered at 2.2 Hz, and digitalized at 20 Hz. No correction was made for liquid junction potential (-3 mV). Cells with more than 20% change in access resistance were discarded. The light-evoked currents were induced at 0.1 Hz (1 ms pulse, 593 nm LED). The A/N ratio was calculated as the amplitude of the AMPA receptor currents recorded at -70 mV divided by the amplitude of the trace at +40 mV 20 ms after the peak. In some recordings, the NMDA receptor currents were blocked using 50 μM D-2-amino-5-phosphonopentanoate (AP-5). The NMDA receptor traces were computed by subtracting the traces recorded at +40 mV in the presence of AP-5 from the traces recorded at +40 mV in the absence of AP-5. The rectification index was calculated as chord conductance at -70 mV divided by chord conductance at +40 mV.

Behavioural protocols

Open field test: The diameter of the round area used for the open field test was 70 cm, and the central zone line was 25 cm from the wall. The mice were placed in the centre of the area at the beginning of the test, and for 10 min their movements were video-recorded and subsequently analysed using ANY-maze 4.7 (Stoelting).

Elevated plus-maze: The elevated plus-maze consisted of two open arms, two closed arms, and a central area elevated to a height of 50 cm above the floor. Mice were placed in the central area and allowed to explore the space for eight minutes.

Repetitive behaviors: The mice were observed for 10 minutes in their home cages equipped with fresh bedding, and the time spent in repetitive behaviors (grooming, digging and jumping) was measured. Grooming was defined as stroking or scratching of the face, head or body with the two forelimbs, or licking the body; digging was defined as the co-ordinated use of both forelimbs or hind legs to dig out or displace bedding materials; jumping was defined as rearing on the hind legs at the corner or along the side walls of the cage, and jumping in such a way as both hind legs are simultaneously off the ground.

Statistical analysis

All of the analyses were made using GraphPad Prism 8.0.2 software. Two sample comparison were made with unpaired t-test if data was normally distributed, and with a non-parametric test if data was not normally distributed. Three groups were analysed with one-way ANOVA followed by Tukey post-hoc test. All of data are expressed as mean values \pm the standard error of the mean (SEM).

Supplementary References

1. Hirrlinger PG, Scheller A, Braun C, Hirrlinger J, Kirchhoff F (2006): Temporal control of gene recombination in astrocytes by transgenic expression of the tamoxifen-inducible DNA recombinase variant CreERT2. *Glia*. 54:11-20.
2. Brenner M, Kisseberth WC, Su Y, Besnard F, Messing A (1994): GFAP promoter directs astrocyte-specific expression in transgenic mice. *J Neurosci*. 14:1030-1037.
3. Narboux-Neme N, Sagne C, Doly S, Diaz SL, Martin CB, Angenard G, et al. (2011): Severe serotonin depletion after conditional deletion of the vesicular monoamine transporter 2 gene in serotonin neurons: neural and behavioral consequences. *Neuropsychopharmacology*. 36:2538-2550.
4. Colin A, Faideau M, Dufour N, Auregan G, Hassig R, Andrieu T, et al. (2009): Engineered lentiviral vector targeting astrocytes in vivo. *Glia*. 57:667-679.
5. Humbel M, Ramosaj M, Zimmer V, Regio S, Aeby L, Moser S, et al. (2021): Maximizing lentiviral vector gene transfer in the CNS. *Gene Ther*. 28:75-88.
6. Petrelli F, Dallerac G, Pucci L, Cali C, Zehnder T, Sultan S, et al. (2020): Dysfunction of homeostatic control of dopamine by astrocytes in the developing prefrontal cortex leads to cognitive impairments. *Mol Psychiatry*. 25:732-749.
7. Zehnder T, Petrelli F, Romanos J, De Oliveira Figueiredo EC, Lewis TL, Jr., Deglon N, et al. (2021): Mitochondrial biogenesis in developing astrocytes regulates astrocyte maturation and synapse formation. *Cell Rep*. 35:108952.
8. Pannasch U, Freche D, Dallerac G, Ghezali G, Escartin C, Ezan P, et al. (2014): Connexin 30 sets synaptic strength by controlling astroglial synapse invasion. *Nat Neurosci*. 17:549-558.
9. Richetin K, Steullet P, Pachoud M, Perbet R, Parietti E, Maheswaran M, et al. (2020): Tau accumulation in astrocytes of the dentate gyrus induces neuronal dysfunction and memory deficits in Alzheimer's disease. *Nat Neurosci*. 23:1567-1579.
10. Schubert V, Bouvier D, Volterra A (2011): SNARE protein expression in synaptic terminals and astrocytes in the adult hippocampus: a comparative analysis. *Glia*. 59:1472-1488.
11. Knott GW, Holtmaat A, Wilbrecht L, Welker E, Svoboda K (2006): Spine growth precedes synapse formation in the adult neocortex in vivo. *Nat Neurosci*. 9:1117-1124.
12. Prada I, Marchaland J, Podini P, Magrassi L, D'Alessandro R, Bezzi P, et al. (2011): REST/NRSF governs the expression of dense-core vesicle gliosecretion in astrocytes. *J Cell Biol*. 193:537-549.
13. Sultan S, Li L, Moss J, Petrelli F, Casse F, Gebara E, et al. (2015): Synaptic Integration of Adult-Born Hippocampal Neurons Is Locally Controlled by Astrocytes. *Neuron*. 88:957-972.